NUREG/CR-3135
LA-9646-MS

Los Alamos National Laboratory is operated by the University of California for the United States Department of Energy under contract W-7405-ENG-36.

Buckling Investigation of Ring-Stiffened Cylindrical Shells with Reinforced Openings under Unsymmetrical Axial Loads

Los Alamos
Los Alamos National Laboratory
Los Alamos, New Mexico 87545

NUREG/CR-3135
LA-9646-MS

R5

Buckling Investigation of Ring-Stiffened Cylindrical Shells with Reinforced Openings under Unsymmetrical Axial Loads

W. Baker*
J. Bennett

Manuscript submitted: December 1982
Date published: February 1983

Prepared for Structural Engineering Branch
Division of Engineering Technology
Office of Nuclear Regulatory Research
US Nuclear Regulatory Commission
Washington, DC 20555

NRC FIN No. A7222

*Visiting Staff Member at Los Alamos. Department of Mechanical Engineering, University of New Mexico, Albuquerque, NM 87106.

Los Alamos Los Alamos National Laboratory
Los Alamos, New Mexico 87545

CONTENTS

FIGURES

BUCKLING INVESTIGATION OF RING-STIFFENED CYLINDRICAL SHELLS WITH REINFORCED OPENINGS UNDER UNSYMMETRICAL AXIAL LOADS

by

W. Baker and J. Bennett

ABSTRACT

Four steel shells having features representative of steel containment vessels for nuclear power plants were fabricated and tested to failure under unsymmetrical axial loading. All of the ring-stiffened shells were 698 mm (27.5 in.) in diam by 0.762 mm (0.030 in.) in wall thickness. Each one had a penetration that was reinforced in accordance with the area-replacement rule of the applicable American Society of Mechanical Engineers (ASME) code and of a design to simulate actual practice for steel containments. The penetrations were of four different diameters, cutting no ring stiffeners, and cutting one, two, and three ring stiffeners. Before testing, imperfections were measured, and strain gages were applied to characterize the strain field at an end and around the penetration. Buckling loads were determined with application parallel to the axis at an eccentricity of R/∂ and were compared with the results from a numerical solution.

I. INTRODUCTION

Steel containment structures for nuclear power plants are subject to loadings postulated to occur as a result of various accidents. Some of these loadings can produce large compressive membrane stresses in local regions of the containment shell. These conditions must be examined for the possibility of failure due to instability in buckling. Computer codes used in such stability analyses require experimental checks of predictive ability. This can be done on models having features typical of those in the actual containment vessel. An experimental program has been conducted to make such checks, and results are described here and in Ref. 1.

The complete experimental program consisted of the design, construction, and testing of six cylindrical, ring-stiffened shells made of steel, and having features representative of steel containments. Two of these six shells did not have penetrations, and the details of the work done on this phase of the overall project are described in Ref. 1. The remaining four shells each had a penetration and reinforcing, and this report describes this phase of the project. As a result of the close relationship between the work done for these two phases of the project, general background material presented in Ref. 1 will not be repeated here. A brief review of works on buckling strengths of shells having penetrations will be given.

The effect of unreinforced penetrations in a shell on the axial buckling strength was studied by Starnes[2] for mylar and copper shells. His work on unstiffened shells showed that when the penetrations are "small," the other initial imperfections control the buckling phenomenon, but that larger penetrations reduce the buckling load. As an example of the degree of reduction, for a penetration approximately the same size as the largest one to be used in this work, Starnes found the buckling load of the mylar cylinder to be reduced by 68% over the buckling load of the unpenetrated cylinder. The R/t ratio of the mylar cylinder used was approximately the same as that used in this work.

Several studies have been made of the effectiveness of restoring the buckling strength to that of the unpenetrated shell with reinforcing. The most pertinent ones to this study are by Miller and Grove[3] and Bennett, et al.[4] Miller and Grove[3] studied the effect on the buckling load of penetrated cylindrical shells of adding reinforcement to the shell wall around a penetration. Mylar shells were used and various amounts of reinforcement were added, up to that required by the area-replacement rule of the ASME code.[5] The results showed that the approximate buckling strength of the unpenetrated cylinder could be restored by reinforcing.

In the work of Bennett et al.,[4] experimental work similar to that of Miller and Grove[3] was done on steel shells. The results were similar in that it was shown that increasing the amount of reinforcement around a penetration could increase the buckling strength, and that it could increase it up to the value for the unpenetrated cylinder. However, it was also shown that for fabricated shells having a penetration of the size used, experimental results could be obtained that showed that neither the penetration nor reinforcement governed the buckling load.

Almroth and Holmes[6] studied the buckling of machined aluminum cylinders having rectangular cutouts, both with and without reinforcement. The R/t ratio was approximately the same as that used in this test series. However, the reinforcement was not typical of containments, and the material behavior was in the elastic range.

A. Problem Statement

Previous experimental studies of the buckling of cylindrical shells under axial loading for which the model design is representative of steel containments have not been made. The design features of interest here include ring stiffening, penetration and reinforcement in accordance with the ASME code, and fabrication by normal shop practices, that is, fabrication without great caution to minimize imperfections. In addition, the question of plastic buckling has not been specifically addressed.

The purpose of this extension to the work of Ref. 1 was to conduct an experimental investigation to determine the buckling strengths of penetrated steel shells having the features typical of steel containments as mentioned above.

Because of the importance of imperfections on the buckling strengths of axially loaded cylindrical shells, the imperfections in the shells tested in this study were measured. The imperfection results will permit assessment of their effect on the buckling response, and will permit evaluation of the quality of the models in terms of the fabrication tolerances for steel containments, as specified in Ref. 5b.

B. Model Description

The construction details of the models tested for this work, excluding the details of the penetrations and added reinforcing, are shown in Fig. 1. This figure is the same as the one for the models used in Ref. 1. The details of the penetrations and reinforcing are given in Figs. 2-5. It should be noted that the penetrations in Models 3-6 cut no ring stiffeners, one ring stiffener, two ring stiffeners, and three ring stiffeners, respectively.

The design of the added reinforcing around the penetration was done by Chicago Bridge and Iron Company and represents industry recommendations as to how it would typically be done on a steel containment structure for a nuclear power plant. The area-replacement method of the ASME code (Ref. 5a) was used as a basis for this design. The code requirement is that the cross-sectional area of the added reinforcing around the hole be at least as great as the cross-sectional area of the removed material, and that specified limits of reinforcement, that is, maximum distances of the reinforcement from the penetration boundaries, be satisfied. Models 3-5 all satisfied the code requirements, with ratios of area added to area removed of 1.08, 1.10, and 1.02, respectively. The corresponding ratio for Model 6 is 0.87.

Model 6 fails to meet the area-replacement rule because of the "limit of reinforcement" requirement in the code that excludes reinforcement from being considered as "area replaced" if it exceeds specified distances both normal to the vessel wall and along the vessel wall. For Model 6, all of the added reinforcement satisfies the "along the vessel wall" requirement, but the "normal to the vessel wall" requirement necessitates excluding the area of enough of the added reinforcement so that the ratio is only 0.87. If all of the reinforcement were included, the ratio of area replaced to area removed would be 1.22.

Similarly, the sizing of the ring stiffeners was also done by Chicago Bridge and Iron Company, also. A check of the ring-stiffener size showed that it satisfies the requirements of Code Case N-284 by a wide margin.

The material used for these models was ASTM steel A-366, the same as used for the baseline benchmarks test series of Ref. 1. Tensile test coupons were cut from the stock of both the 0.762-mm- (0.030-in.-) and 3.05-mm- (0.120-in.-) thick material in the transverse and longitudinal directions, and tests were conducted to determine the uniaxial stress-strain curves of the material. These tests were conducted on a 88-kN (20 000-lb) Instron testing machine. Strains in the test specimen were based upon measurements made with a strain gage extensometer. Three specimens for each material thickness and direction were tested. Figures 6 and 7 show the results of these tests for a specimen of each thickness. Table I summarizes the values for the modulus of elasticity and the 0.2% offset-yield stress.

Figures 8-11 are photographs showing the exterior details of the four models, and Figs. 12-15 are photographs that show the interior reinforcement.

TABLE I

ELASTIC MODULUS AND YIELD STRENGTH

Specimen Direction	Average Elastic Modulus (psi)	(GPa)	Average Offset Yield Strength (psi)	(MPa)
Nominal Material Thickness 0.762 mm (0.30 in.)				
Longitudinal	29.0×10^6	200	31 200	215
Transverse	29.8×10^6	206	32 100	221
Nominal Material Thickness 3.05 mm (0.120 in.)				
Longitudinal	29.4×10^6	203	28 700	198
Transverse	33.3×10^6	230	35 000	241

C. Imperfection Measurements and Results

Imperfection measurements were made on these four models. Linear Variable Differential Transformers (LVDTs) were used to measure radial variations in the contour as the model was slowly turned. The equipment and software developed for the work of Ref. 1. were used. It was necessary to develop a special test technique to handle the areas at and near the penetrations. The assumptions made for data reduction and the data-reduction method were, in essence, the same as those used and reported in Ref. 1.

The plots of the imperfections for each of the four models in this series are shown in Figs. 16-19.

These data were analyzed further to determine whether the models would satisfy the criterion on diameter variation as specified in section NE-4221.1 of Ref. 5b. The code states that "the difference between the maximum and minimum inside diameter at any cross section shall not exceed 1% of the nominal diameter at the cross section under consideration....When the cross section passes through an opening, the permissible difference in inside diameters...may be increased by 2% of the inside diameter of the opening."[5b] Table II shows the results of the application of this criterion.

This table shows that each of the models easily satisfies this code-required tolerance.

In addition to the LVDT measurements, chord-gage measurements of the type described in Ref. 1 were made on Model 4 of this series. Further studies of

TABLE II

MODEL DIAMETER VARIATION

Model	Worst Cross Section	Maximum Diameter (in.)	Maximum Diameter (mm)	Minimum Diameter (in.)	Minimum Diameter (mm)	Difference (%)
3	41	27.517	698.93	27.479	697.97	0.14
4	12	27.504	698.60	27.417	696.39	0.32
5	2	27.505	698.63	27.445	697.10	0.22
6	48	27.524	699.11	27.449	697.20	0.27

chord-gage data-reduction methods to obtain results in a form equivalent to the imperfection measurements mentioned above are in progress. Results of these studies will be given in a subsequent report.

D. Test Procedure

After completion of the measurement of the imperfections in each model, we applied strain gages to accomplish two objectives. First, strain gages were applied around each model at a cross section near the lower ring to give information on the strain distribution near the end of the shell. Second, gages were applied on the body of the model in the area in which the initial buckle was most likely to occur. Gages were applied on the inside and outside surface at all locations so it would be possible to separate membrane and bending strains. Both single-element gages and three element rosettes were used, each having a 1.52-mm (0.06-in.) gage length. The locations of the gages and rosettes on Models 3-6 are given in Figs. 20-23, respectively.

During a test, each of the strain gages was placed in a separate bridge circuit and power to the bridge was supplied continuously. Output voltage of each bridge during a test was measured and recorded during repetitive scans with a Hewlett Packard 3054 DL data-acquisition system. Calibration of each bridge was accomplished by placing a calibration resistor in parallel with the active leg. During a test, scans to measure the output voltage of the bridges were initiated every 20 s.

The tests were conducted on a 55 kip (200 kN) servohydraulic testing machine. The machine and hardware used were the same as that used for the tests of Ref. 1. Figure 24 is a sketch of the model and loading hardware.

The test procedure was essentially the same also. First, during the process of placing the test model in the machine, the space between the ends of the model and the end plates was filled with epoxy. A central load of 8.9 kN (2000 lb) was placed on the assembly during the curing of the epoxy. The purpose of the epoxy filler was to accomplish in the experiment, as well as possible, uniform support around the ends of the model.

The first test on each model was with central loading. The load was applied slowly to 44.5 kN (10 000 lb), and during the loading process, repetitive scans of all channels of instrumentation were made and recorded. After completion of a scan at 44.5 kN (10 000 lb), we removed the load and took a final scan.

After reviewing the data to check for errors, open channels, etc., and making adjustments where necessary, we moved the test model and end plates from the center load position to the R/2 offset position as shown in Fig. 24. Figure 25 shows a model in this position before testing.

Displacement control was used on the hydraulic ram of the testing machine during all tests. With this type of loading, the buckles, once initiated, could be observed while forming, and the loading process terminated before excessive deformations occurred. Buckling was identified as the maximum compressive load that the shell would support.

E. Results

Results obtained from the load tests on each model included the buckling load, load-strain curves for each gage element, a load-time curve, and a load-ram stroke curve. Presentation of all of these results in this report is not practical, but all will be kept available for future reference. Only brief, selected results will be presented here.

F. Model 3

The readings from the strain gages around the base of the model for a compressive load of 44.5 kN (10 000 lb) are plotted in Fig. 26 for both the axisymmetric load and the eccentric load. For the axisymmetric load, the uniformity of the loading is less than desirable but is judged acceptable.

While the curve for the eccentric load shows the higher strains at the location affected by the eccentric load, it also does not have the expected shape exhibited by the baseline benchmark cylinders of Ref. 1.

The buckling load was 133.9 kN (30 110 lb). Figures 27 and 28 show the deformation immediately after buckling. Two modes are observed, the first one, a (near) diamond pattern between ring stiffeners and the second, an axisymmetric buckle across a ring stiffener for which the shell cross section at the buckle had an "S" shape. The ring stiffeners involved had permanent torsional deformation. This type of axisymmetric mode occurred on one of the baseline benchmark models also.[1] Although it is highly probable that one of the two buckling modes seen occurred first, with the resulting deformation triggering the second, which mode occurred first was not determined.

The performance of this model shows that the presence of the reinforced penetration had minimal effect on the buckling load. This is in substantial agreement with Meller and Bushnell[7] whose analysis showed a buckling load of 120.3 kN (27 040 lbs). This predicted buckling load is less than 1% below their predicted load for the unpenetrated configuration. The buckling contours predicted by Meller and Bushnell for this model are shown in Fig. 29. Discrepancies can be partly attributed to the imperfections in the model, which were not considered in the analysis.

G. Model 4

The measured strain distribution around the base of Model 4, at a load of 44.5 kN (10 000 lb) is shown in Fig. 30. The strain distribution for the axisymmetric loading is nearly uniform around the lower edge, as would be expected for this type of load. The corresponding strain distribution for a 44.5-kN (10 000-lb) eccentric load shows the expected symmetry and the higher strains in the direction of the eccentricity.

The measured buckling load was 97.4 kN (21 900 lb). The buckled configuration is shown in Figs. 31 and 32. The load computed for this model by Meller and Bushnell[7] was 103.6 kN (23 200 lb), and the buckling contours from their analysis are shown in Fig. 33. A comparison of actual buckling contours with the computed one shows certain differences. The diamond buckle pattern in the model is in the uppermost 63.5-mm- (2.5-in.-) wide bay. The analysis shows the deepest buckle to be in the 63.5-mm- (2.5-in.-) wide bay immediately above the penetration. However, when the location of the buckles is not considered and only the actual contours are, there is remarkably good agreement between the actual and computed buckling contour.

The probable reason for the disagreement can be identified by a study of Fig. 17, the plot of imperfections in Model 4. Three imperfections best described as "dents" have been identified with the Nos. 1-3. These imperfections were studied before the buckling test, and it was noted that dent 1 appeared to be the result of a crease and of a failure of the solder joint between the adjacent ring stiffener and the shell body. This imperfection was repaired. Imperfections 2 and 3 were not repaired. Their influence on buckling was apparently significant, since the model buckled at each of these imperfections. It also buckled at a load that was 6% less than the computed load.

H. Model 5

Figure 34 shows the strain distribution around the model near the lower end, for a load of 44.5 kN (10 000 lb) applied both symmetrically and unsymmetrically. For the unsymmetric load, there is an indication that there is a perturbation in the expected uniform distribution underneath the penetration.

The buckling load for Model 5 was 94.2 kN (21 170 lb) and the buckling deformation is shown in Figs. 35 and 36. As with Model 4, the failure was localized, with an inward, diamond type of buckle.

The buckling load computed by Meller and Bushnell[7] for this model was 94.9 kN (21 340 lb) and the buckling contours determined from their numerical work are shown in Fig. 37.

The difference between the measured and computed buckling load for this model was only 0.8%, and the locations and types of the actual and measured buckle contours were in agreement. These results are considered excellent.

I. Model 6

The strain distributions near the base of Model 6 at loads of 44.5 kN (10 000 lb) are shown in Fig. 38. For the case where the load was at the center, there was a significant deviation from uniform distribution underneath the penetration. This shows that a penetration this size, even with the reinforcement around it that is essentially in accordance with the ASME area replacement rule, will distort the strain field a significant distance from the penetration. The same type and degree of deviation from the expected distribution occurs even with the eccentric load.

The buckling load for Model 6 was 82.6 kN (18 560 lb), and the buckled configuration is shown in Figs. 39 and 40. Although the buckling deformation on this model, as seen in these figures (and the other models as well), is small, it must be remembered that the use of displacement controls on the ram made it possible to limit the deformation, thus eliminating large postbuckling deformations.

The buckling load computed by Meller and Bushnell[7] was 94.2 kN (21 180 lb). The measured load was 12.4% below this valve. However, their predictions for the type and location of the buckles were in substantial agreement with the test results. Figure 41 shows their predicted buckling contours.

II. SUMMARY

Table III summarizes the results of the tests on the six ring-stiffened cylinders of Ref. 1 and this report. There are several significant conclusions from this test series and the analysis of Ref. 7 and these are given below.

1. The tests and analysis show that circular penetrations in cylindrical shells that have containment-like features will reduce the axial buckling load, even though the penetrations are reinforced in accordance with the area-replacement method of the ASME code.
2. The analysis technique of Meller and Bushnell gives excellent results for the buckling loads for these geometries. This was the case even though two of the six models failed with an S-shaped buckling deformation, a mode not predicted by analysis.
3. Imperfections in shells having ring stiffeners designed to satisfy Code Case N-284 of the ASME code 5c apparently have minimal effect on the buckling load. Further study of this area is required.

TABLE III
RESULTS OF BENCHMARK TESTS

Model No.	Penetration Data (in.)	Buckling Load (lb) Predicted	Measured	Difference (%)	Type of Buckle
1	--	27 090	23 300	-14.0	Elephant Foot
2	--	27 090	26 910	- 0.7	S Type
3	1.5	27 040	30 110	+11.4	Local and S Type
4	4.0	23 300	21 900	- 6.0	Local
5	6.5	21 340	21 171	- 0.8	Local
6	9.0	21 180	18 560	-12.4	Local

REFERENCES:

1. J. G. Bennett, W. E. Baker, and C. D. Babcock, "Buckling Investigation of Ring Stiffened Shells Under Unsymmetrical Axial Loads." Los Alamos National Laboratory report LA-9536-MS (October 1982).

2. J. H. Starnes, "The Effect of Cutouts in the Buckling of Thin Shells," Thin-Shell Structures - Theory, Experiment, and Design, Y. C. Fung and E. E. Sechler, Eds. (Prentice Hall Inc., Englewood Cliffs, New Jersey, 1974) pp. 289-304.

3. C. D. Miller and R. B. Grove, "Buckling of Cylindrical Shells with Reinforced Circular Openings Under Axial Compression," Chicago Bridge and Iron Company report (March 14, 1980).

4. J. G. Bennett, R. C. Dove and T. A. Butler, "An Investigation of Buckling of Steel Cylinders with Circular Cutouts Reinforced in Accordance with ASME Rules," Los Alamos National Laboratory report LA-8853-MS (June 1981).

5. ASME Boiler and Pressure Vessel Code, Section III, Nuclear Power Plant Components, Division 1, Subsection NE, 1977 edition,
   a. Article 3000. Design.
   b. Article 4000. Fabrication and Installation.
   c. Code Case N-284 Metal Containment Shell Buckling.

6. B. O. Almroth and A. M. C. Holmes, "Buckling of Shells with Cutouts, Experiment and Analysis," Int. J. of Solids Structures, 8, 1057-1071 (1972).

7. E. Meller and D. Bushnell, "Elastic-Plastic Collapse of Nonuniformly Axially Compressed Ring-Stiffened Cylindrical Shells with Reinforced Openings," Lockheed Missile and Space Company, NUREG/CR-2836 (1982).

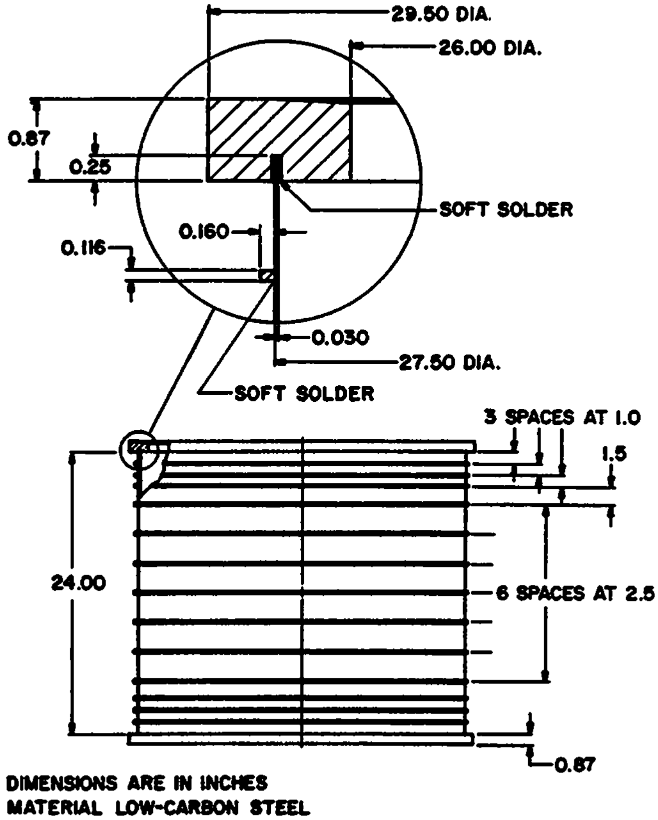

Fig. 1. Model detail, excluding penetration.

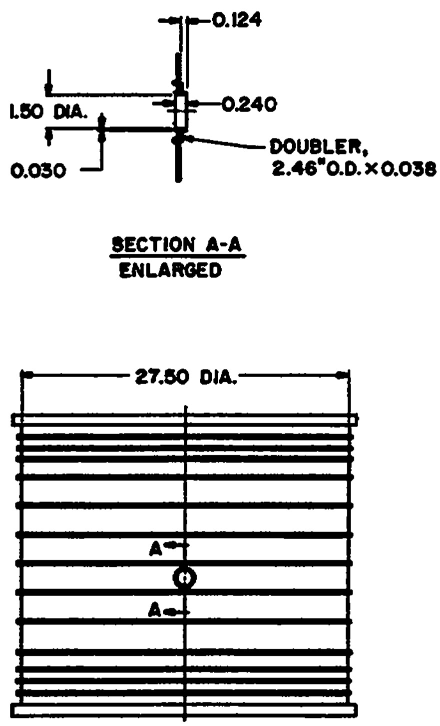

Fig. 2. Model 3 penetration and reinforcement details.

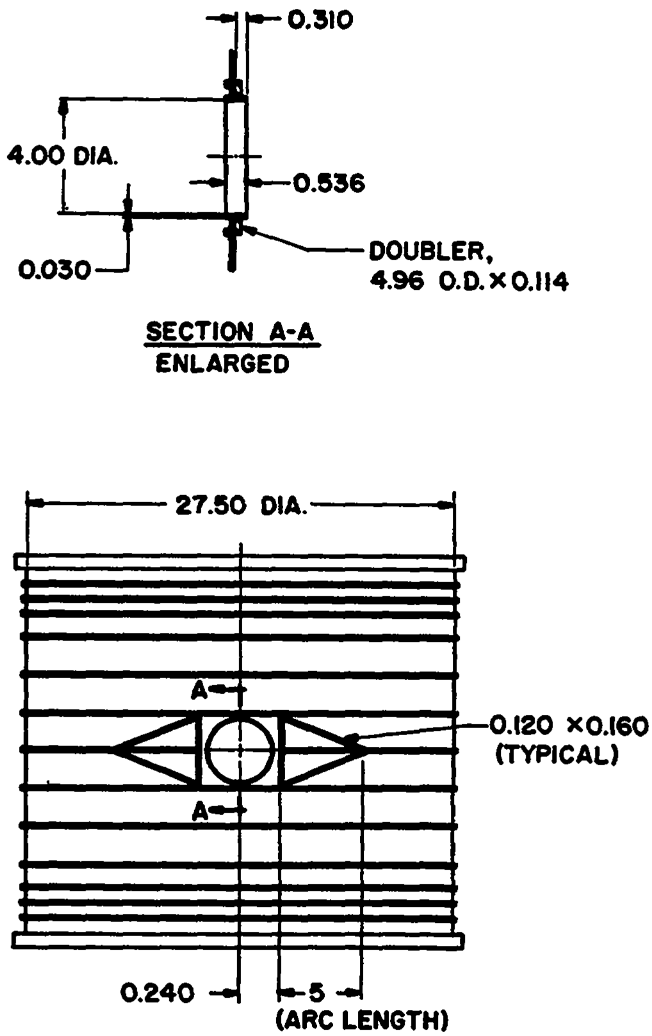

Fig. 3. Model 4 penetration and reinforcement details.

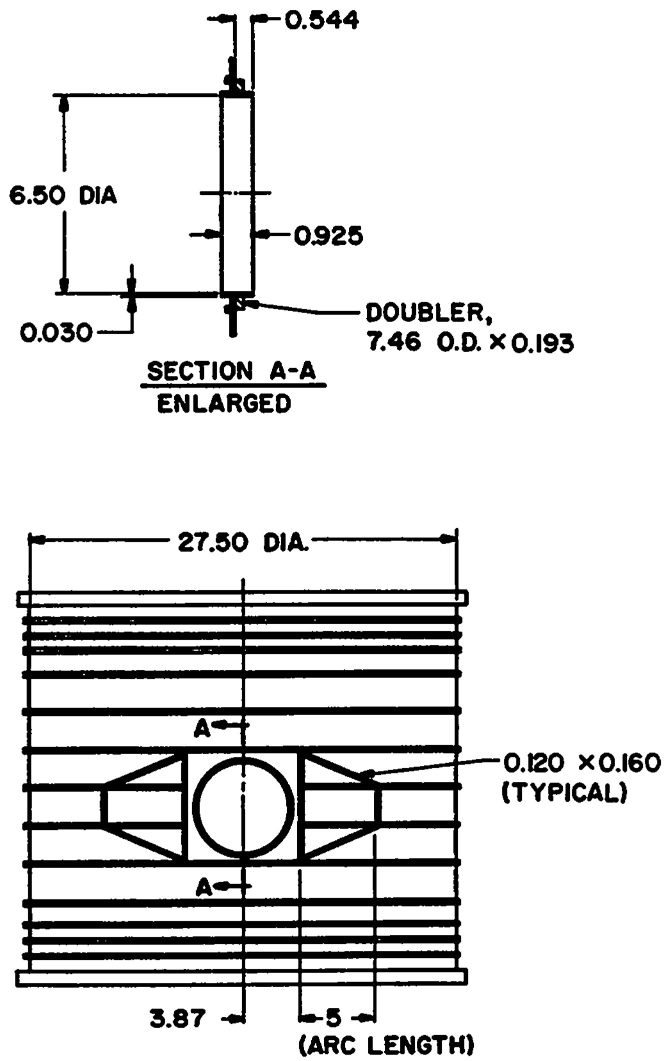

Fig. 4. Model 5 penetration and reinforcement details.

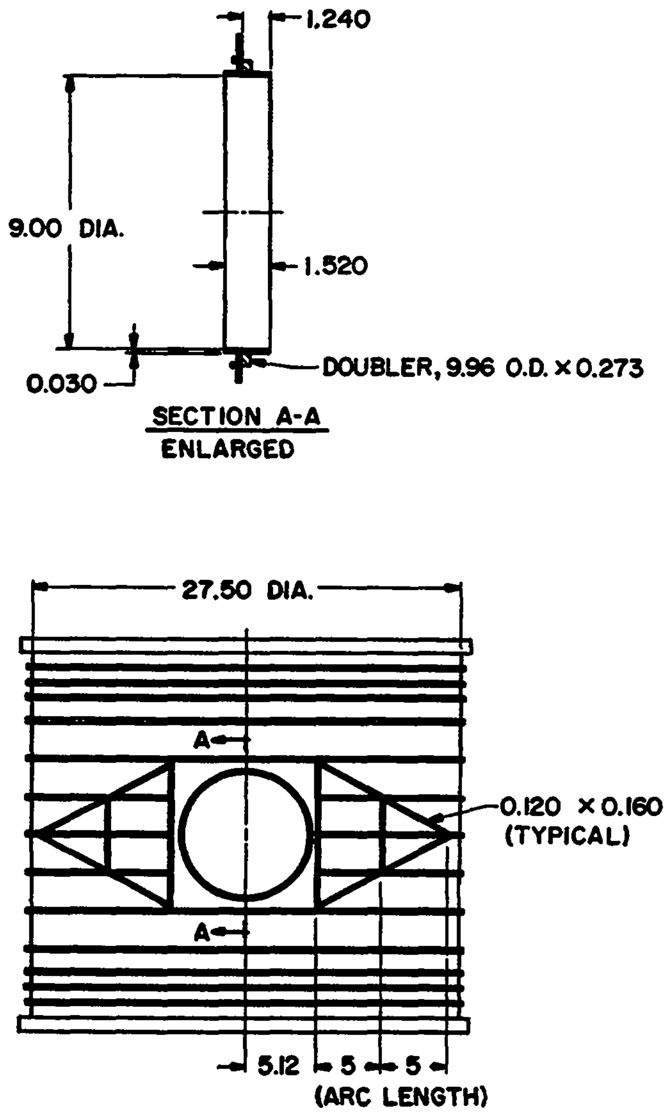

Fig. 5. Model 6 penetration and reinforcement details.

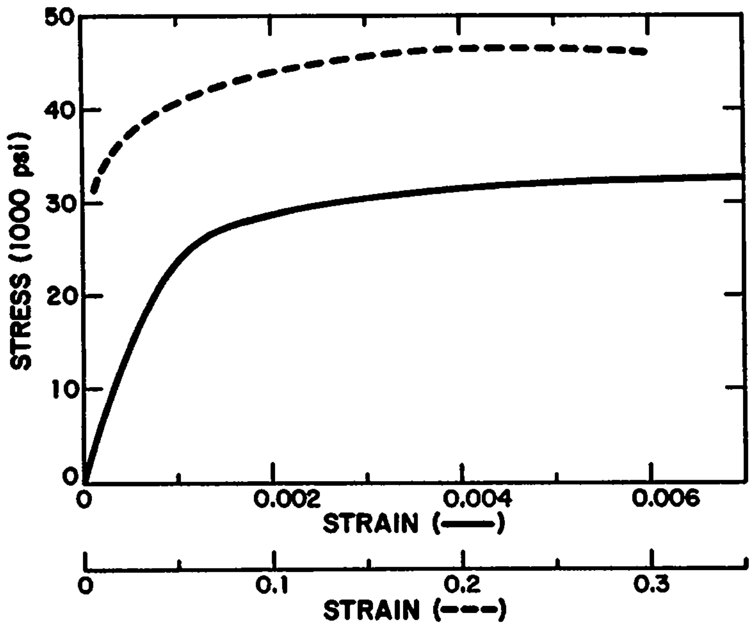

Fig. 6. Stress-strain curve for the shell material.

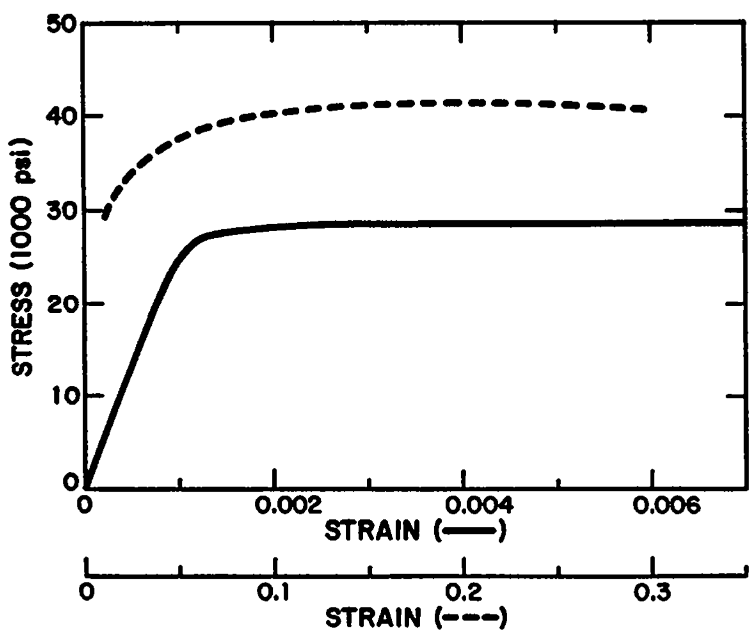

Fig. 7. Stress-strain curve for the ring-stiffener material.

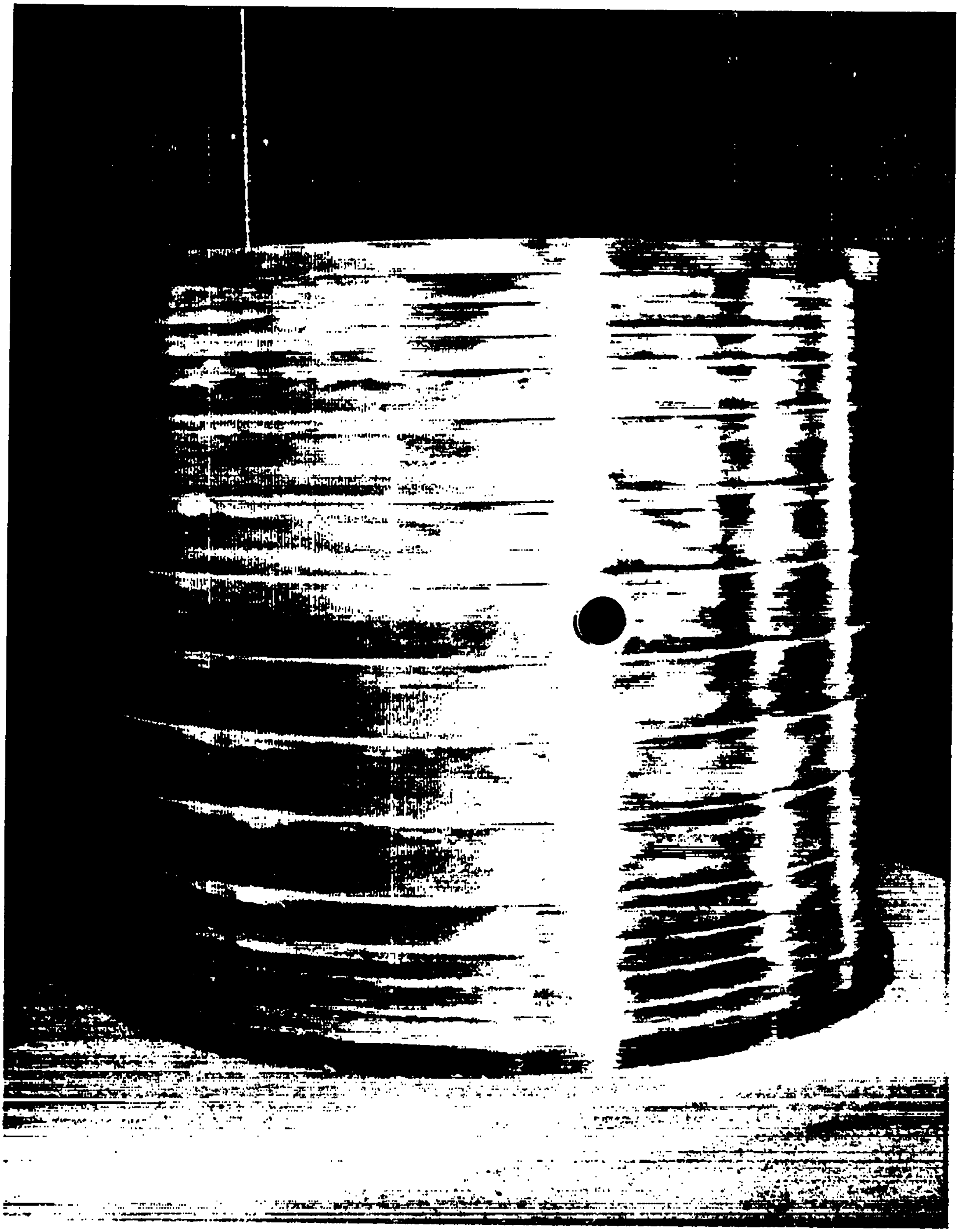

Fig. 8. Model 3.

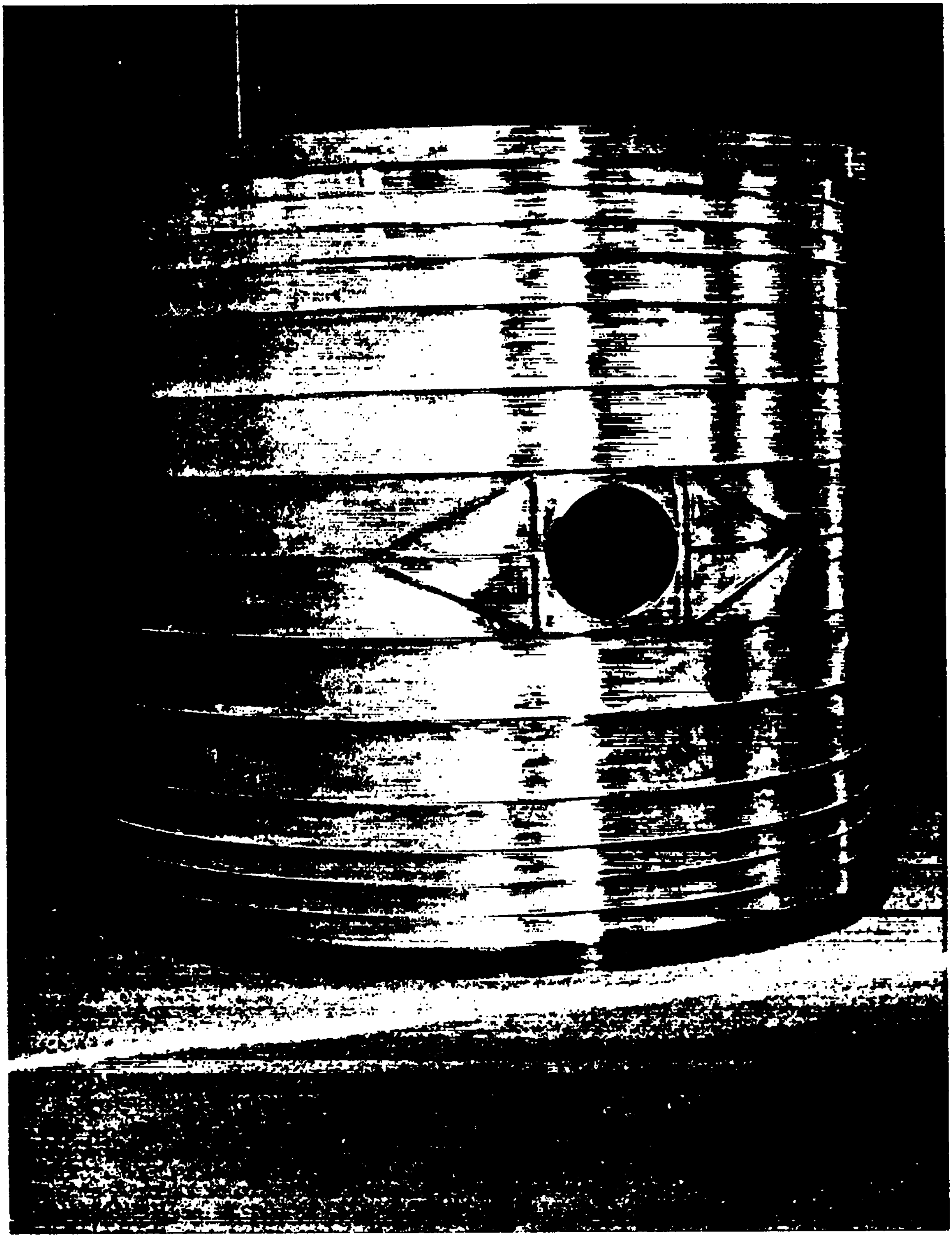

Fig. 9. Model 4.

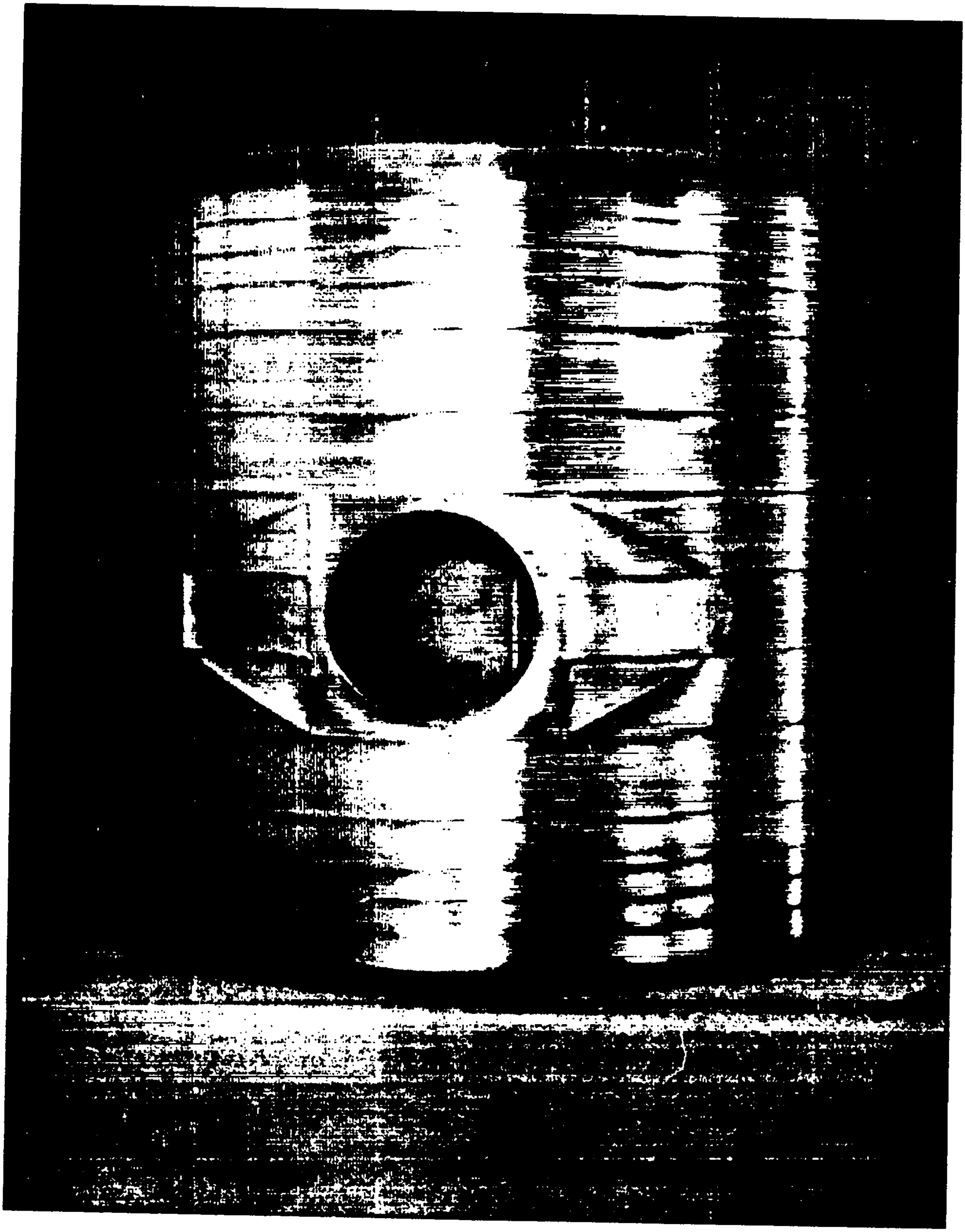

Fig. 10. Model 5.

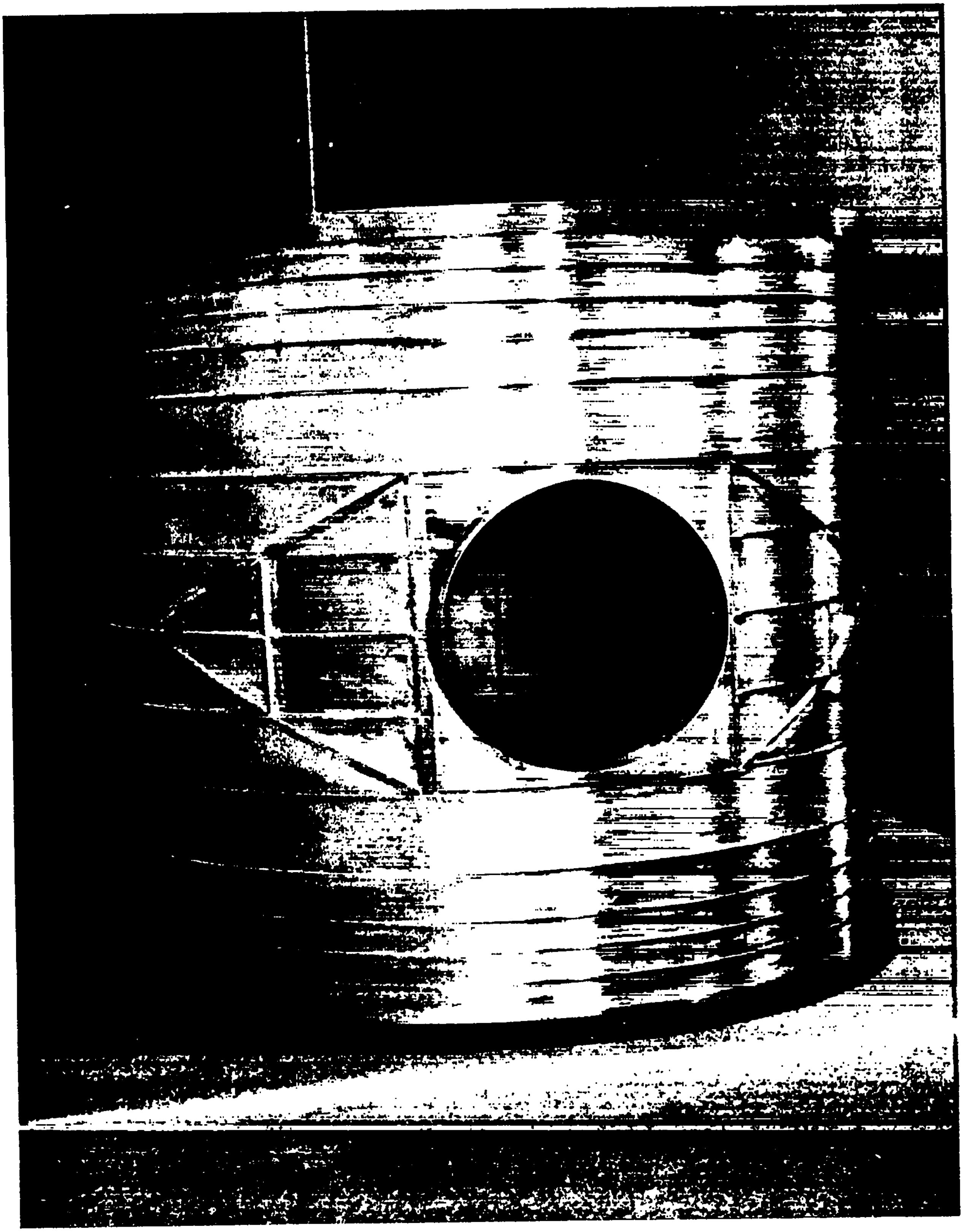

Fig. 11. Model 6.

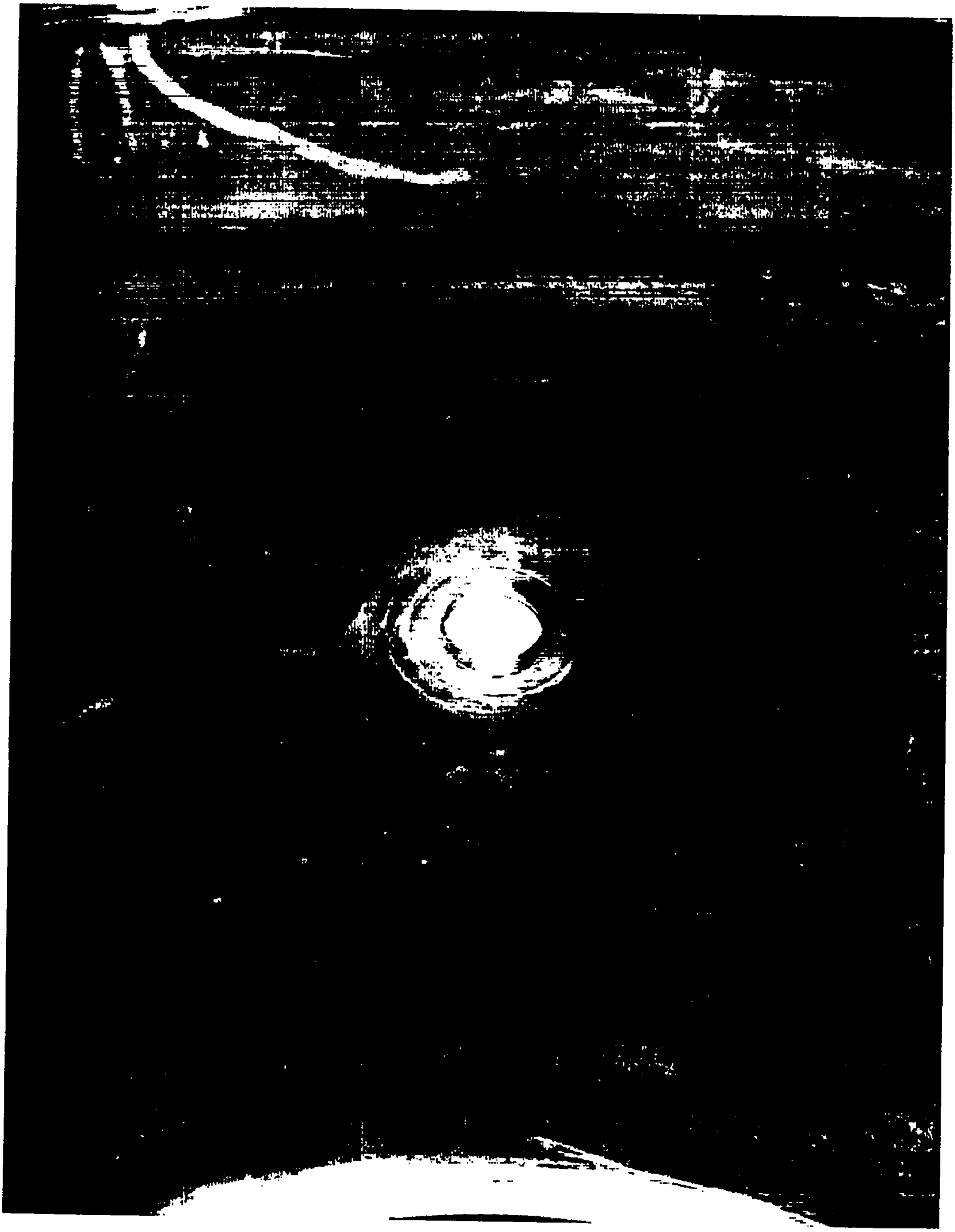

Fig. 12. Interior reinforcement on Model 3.

Fig. 13. Interior reinforcement on Model 4.

Fig. 14. Interior reinforcement on Model 5.

Fig. 15. Interior reinforcement on Model 6.

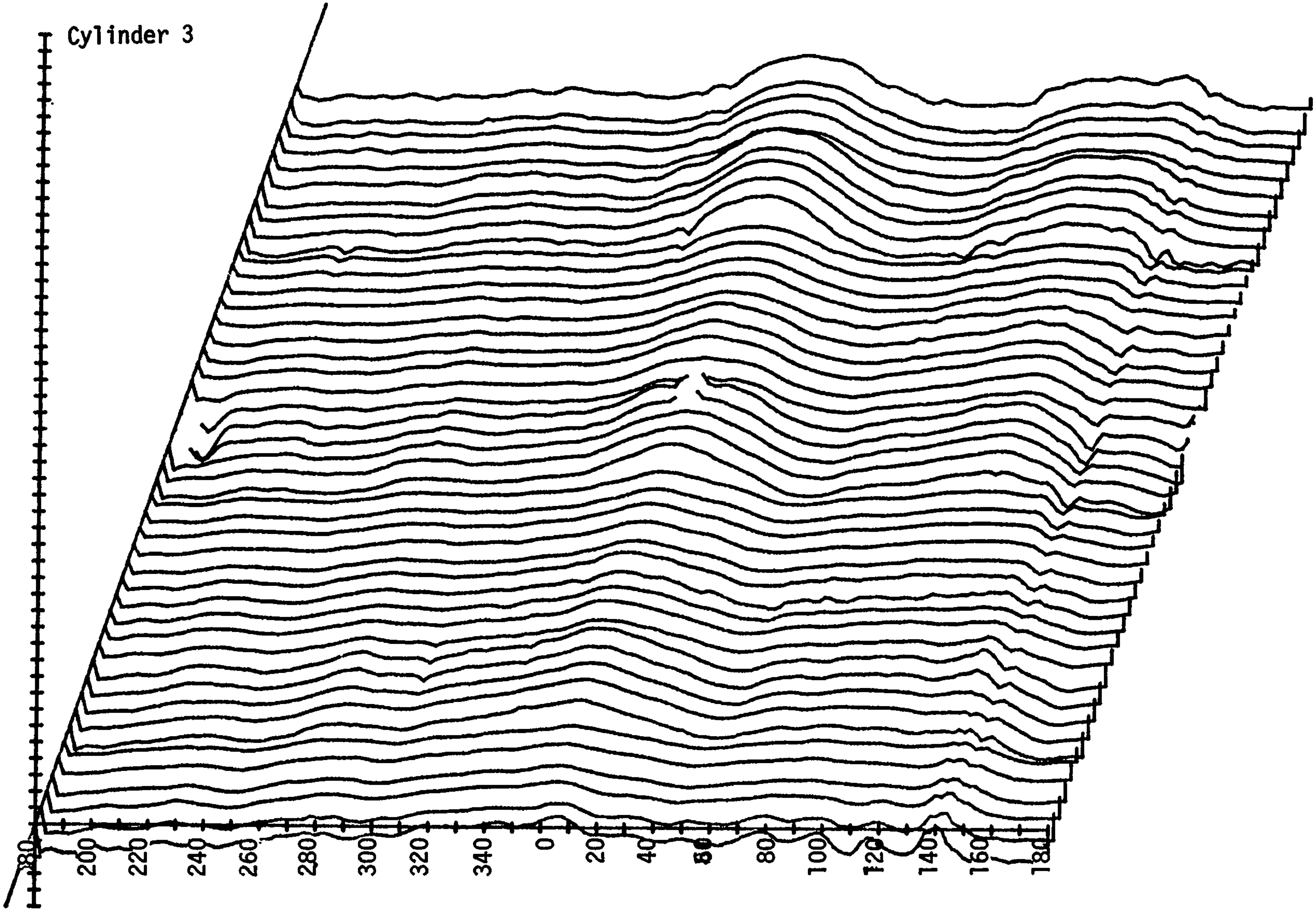

Fig. 16. Model 3 imperfection plot.

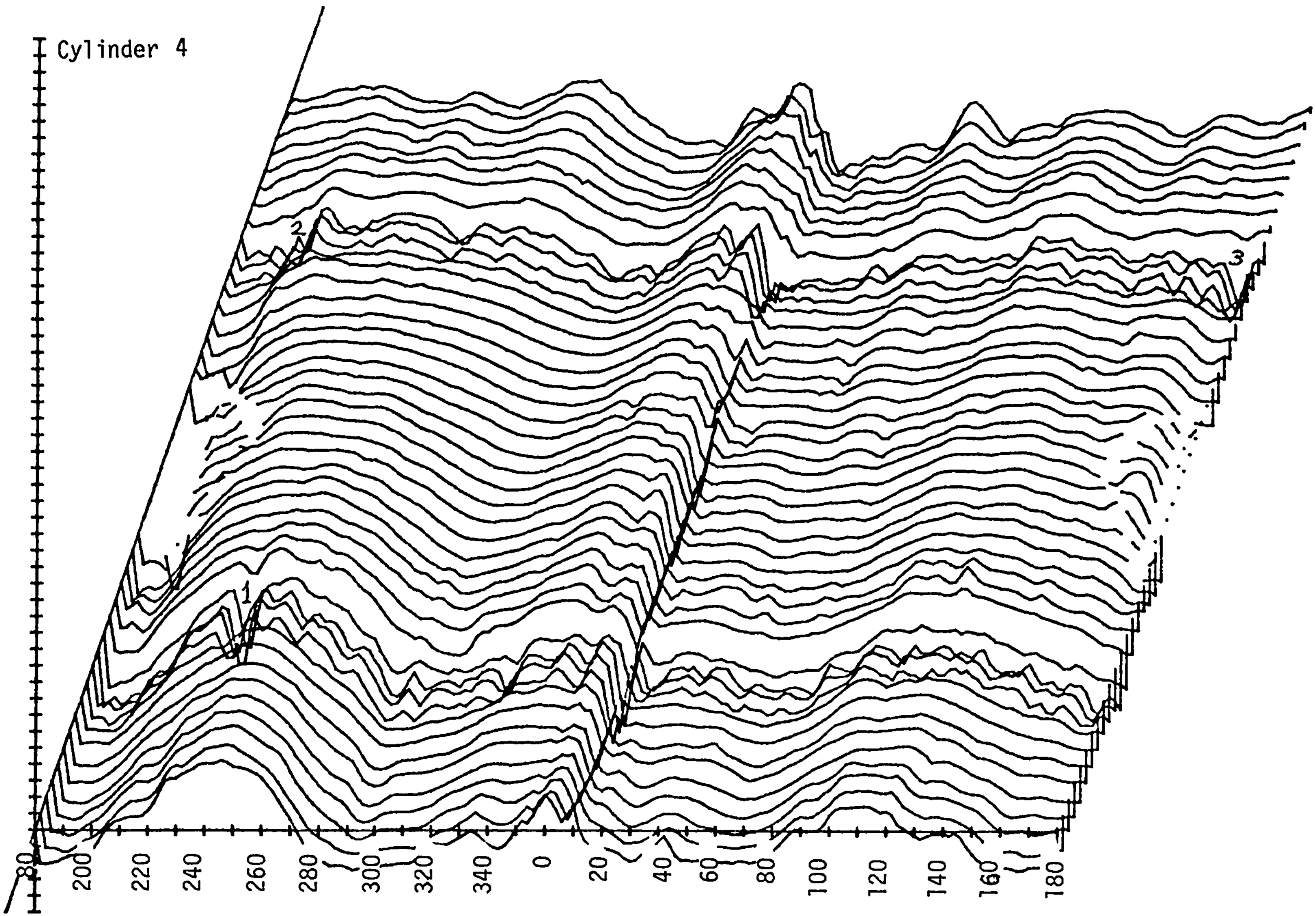

Fig. 17. Model 4 imperfection plot.

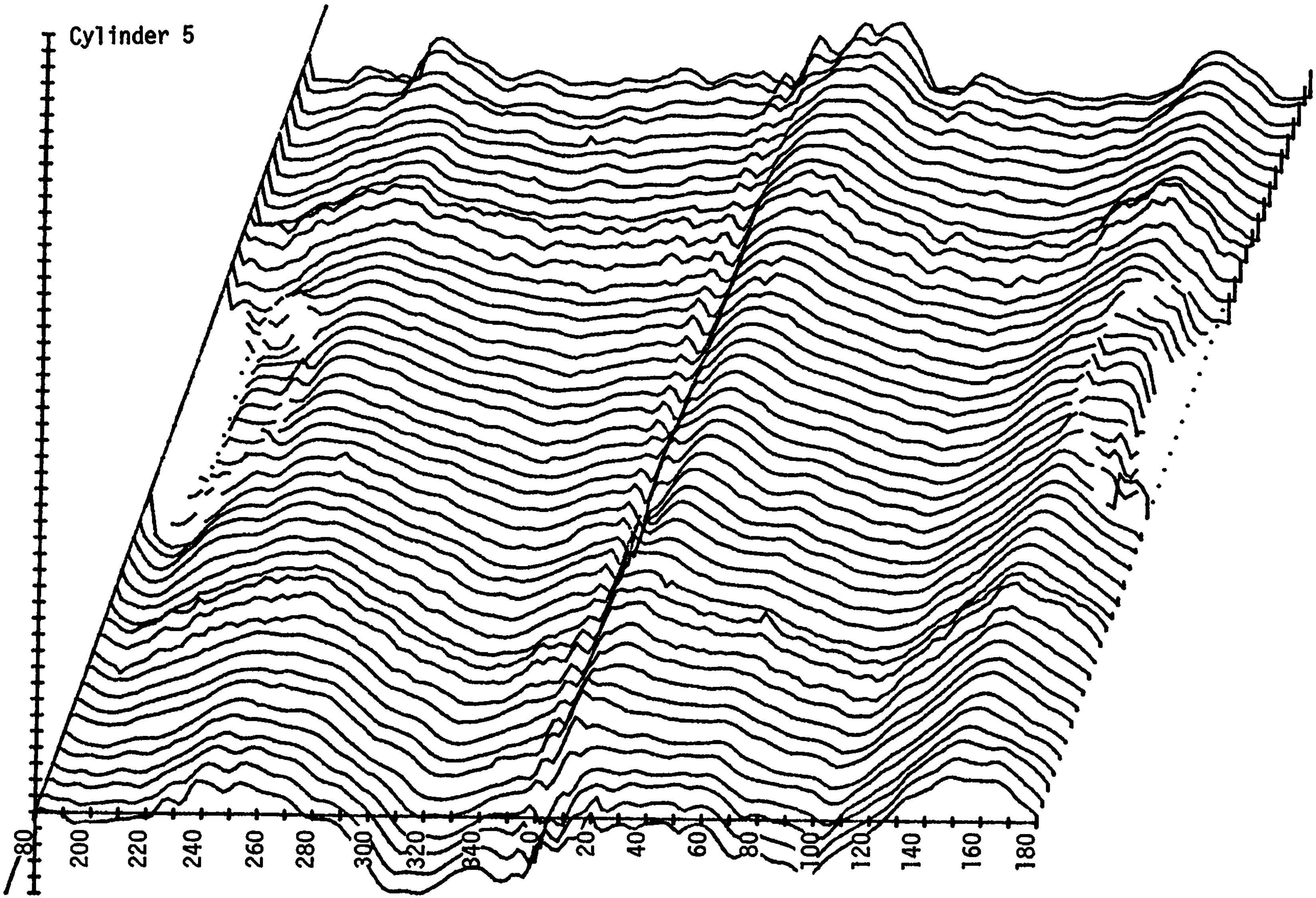

Fig. 18. Model 5 imperfection plot.

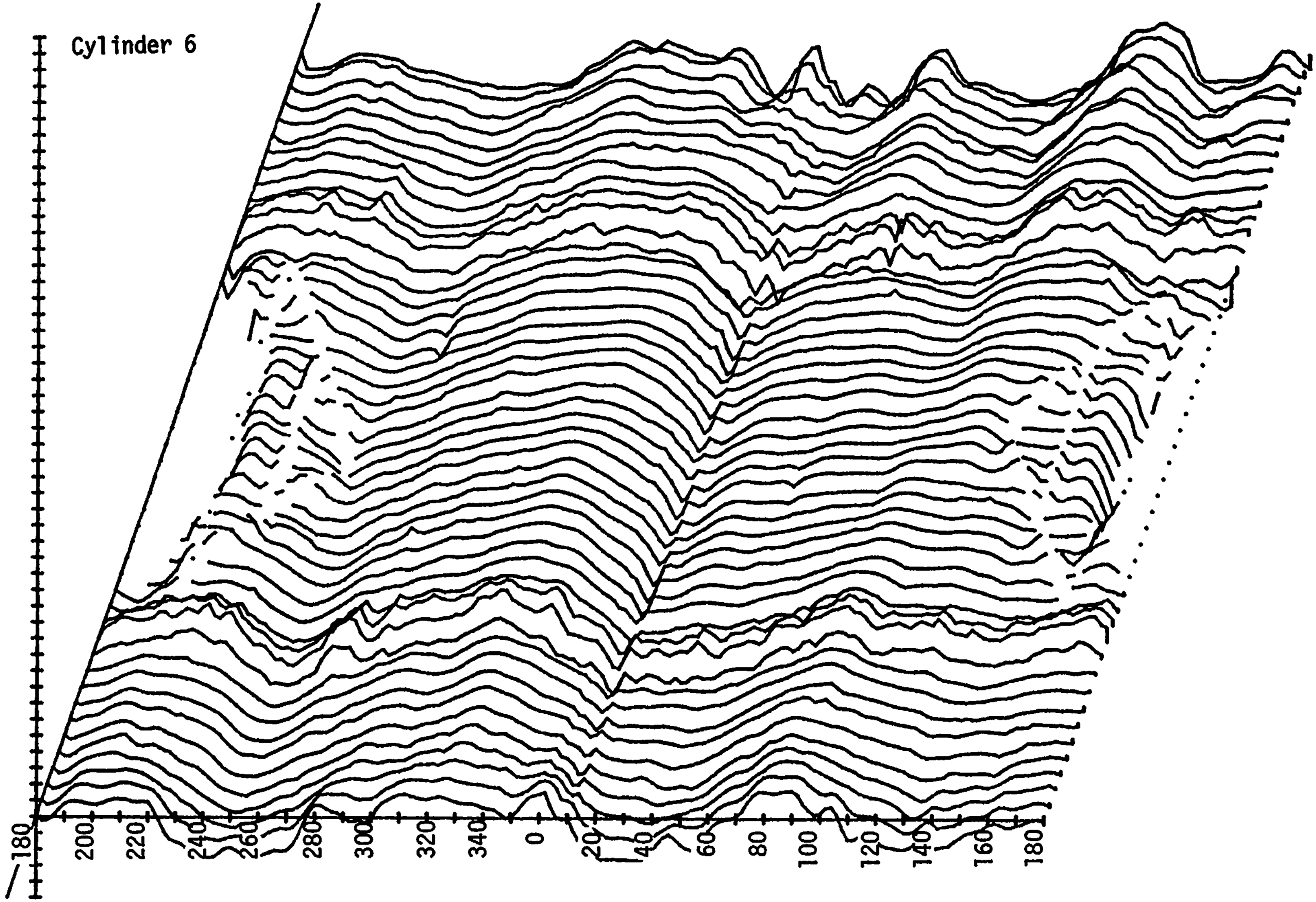

Fig.19. Model 6 imperfection plot.

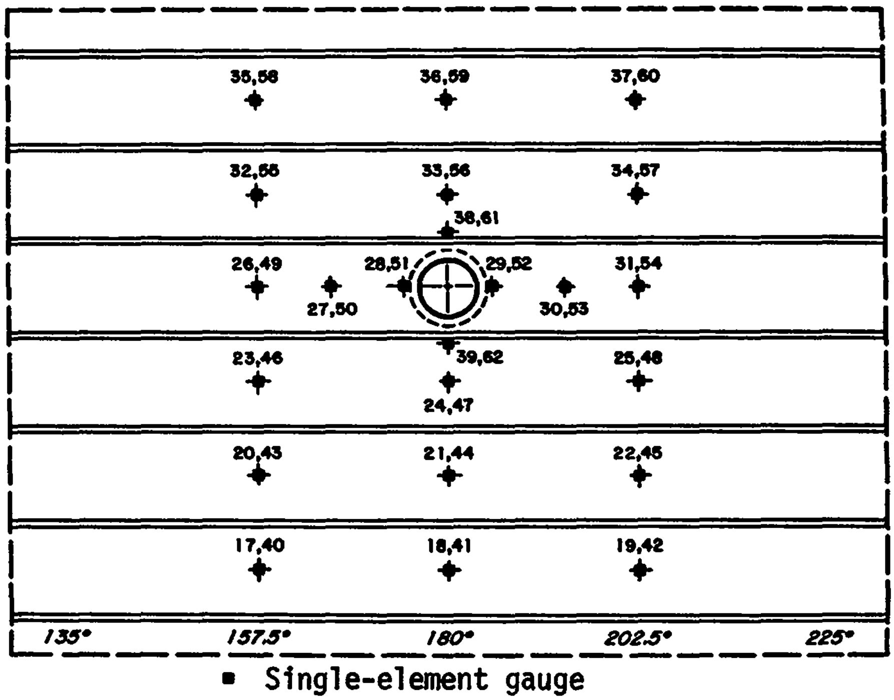

Fig. 20. Strain-gage locations on Model 3.

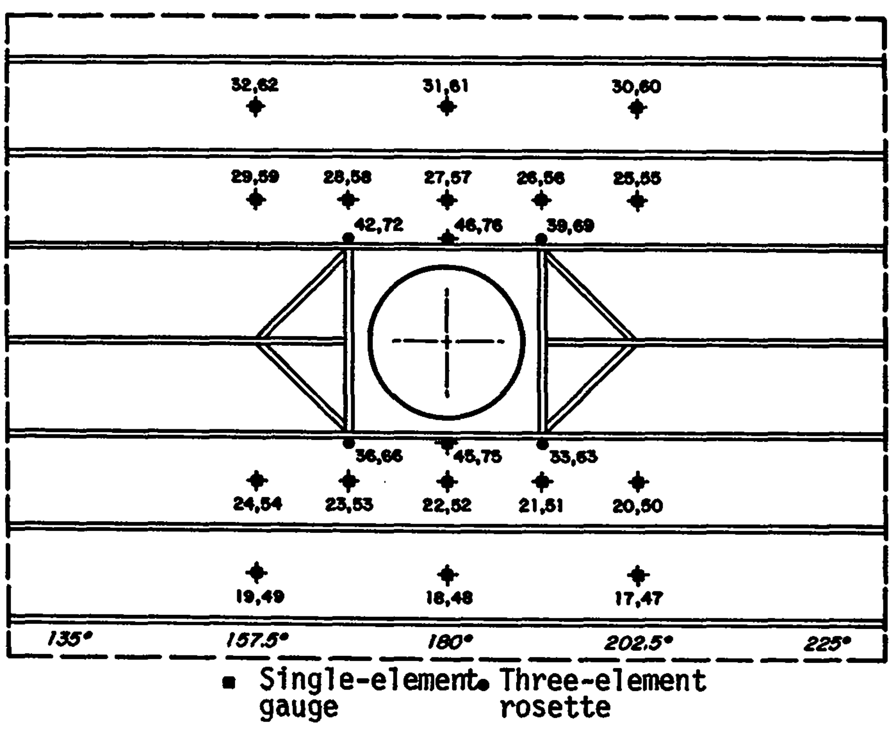

Fig. 21. Strain-gage locations on Model 4.

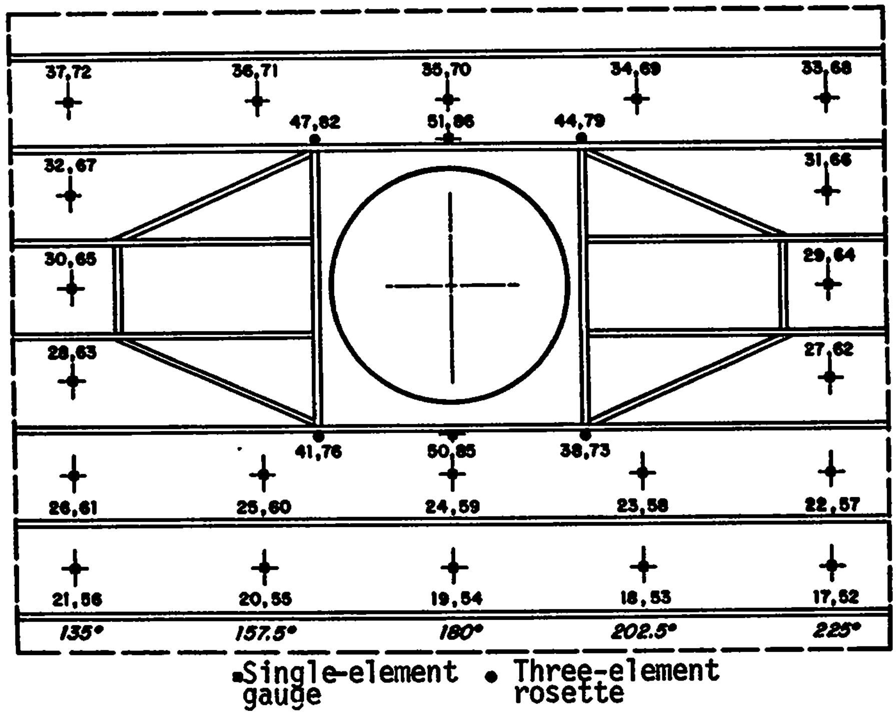

Fig. 22. Strain-gage locations on Model 5.

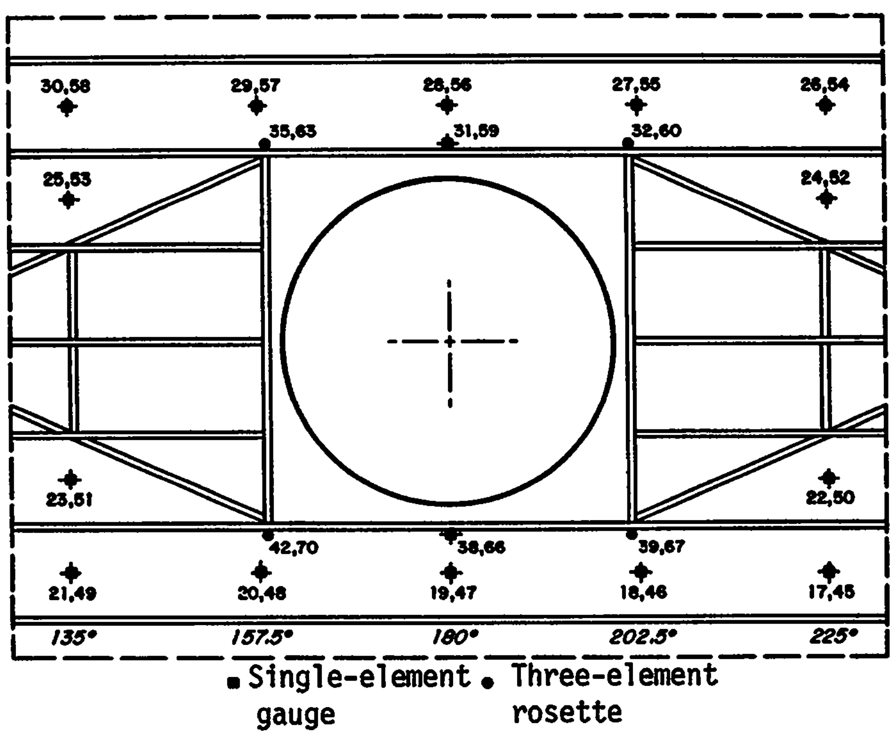

Fig. 23. Strain-gage locations on Model 6.

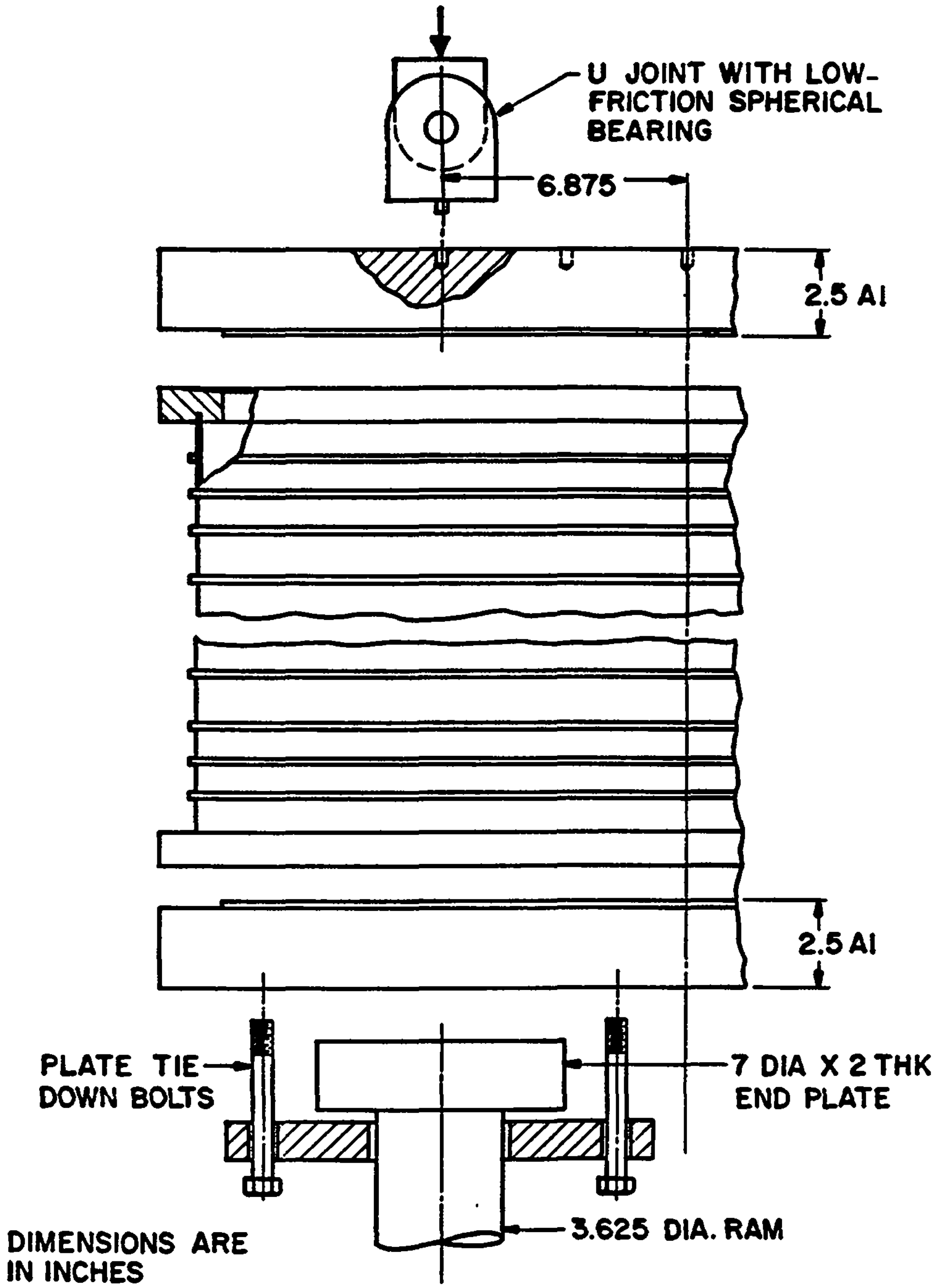

Fig. 24. Model and loading hardware.

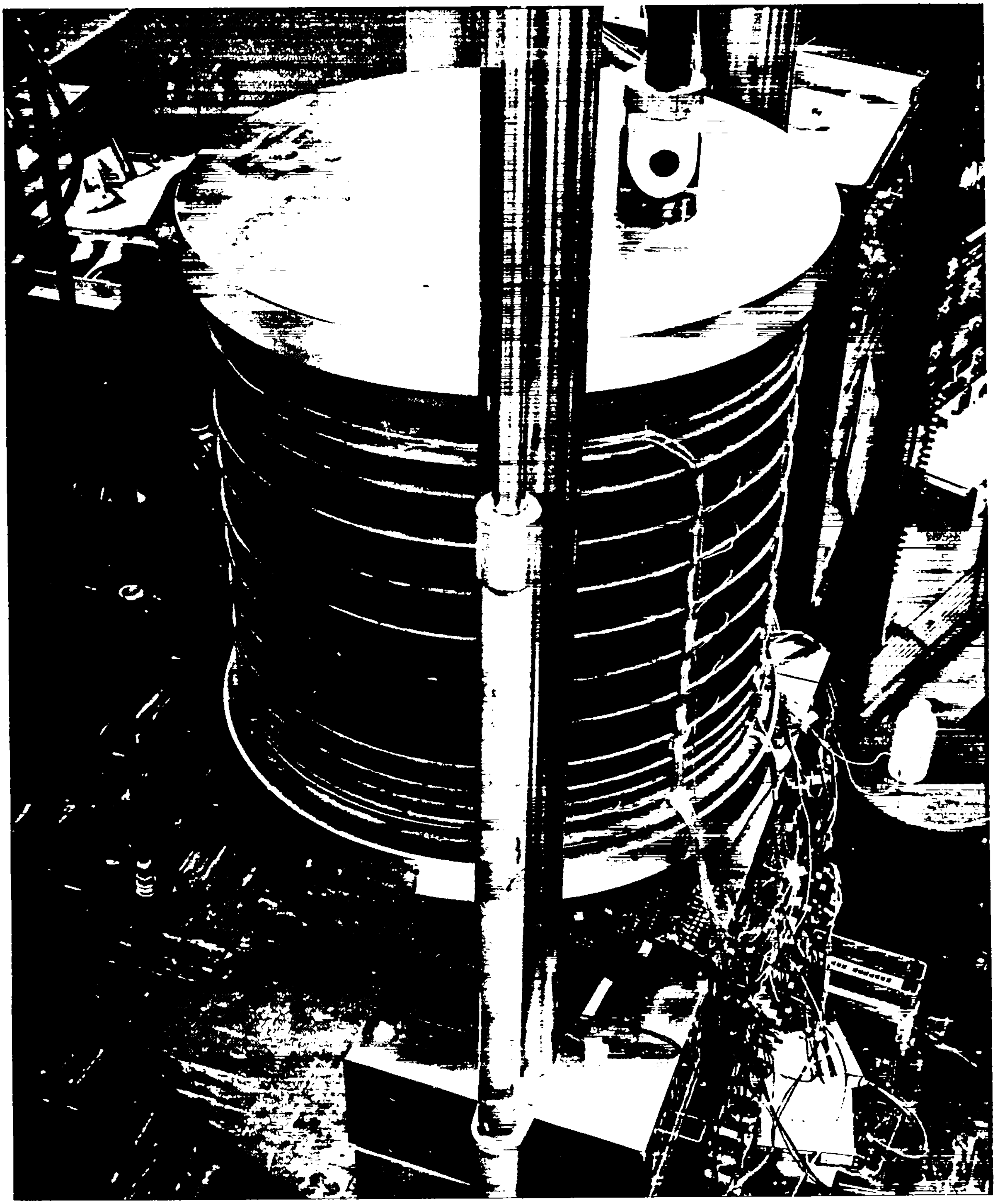

Fig. 25. Top view of model in loading machine.

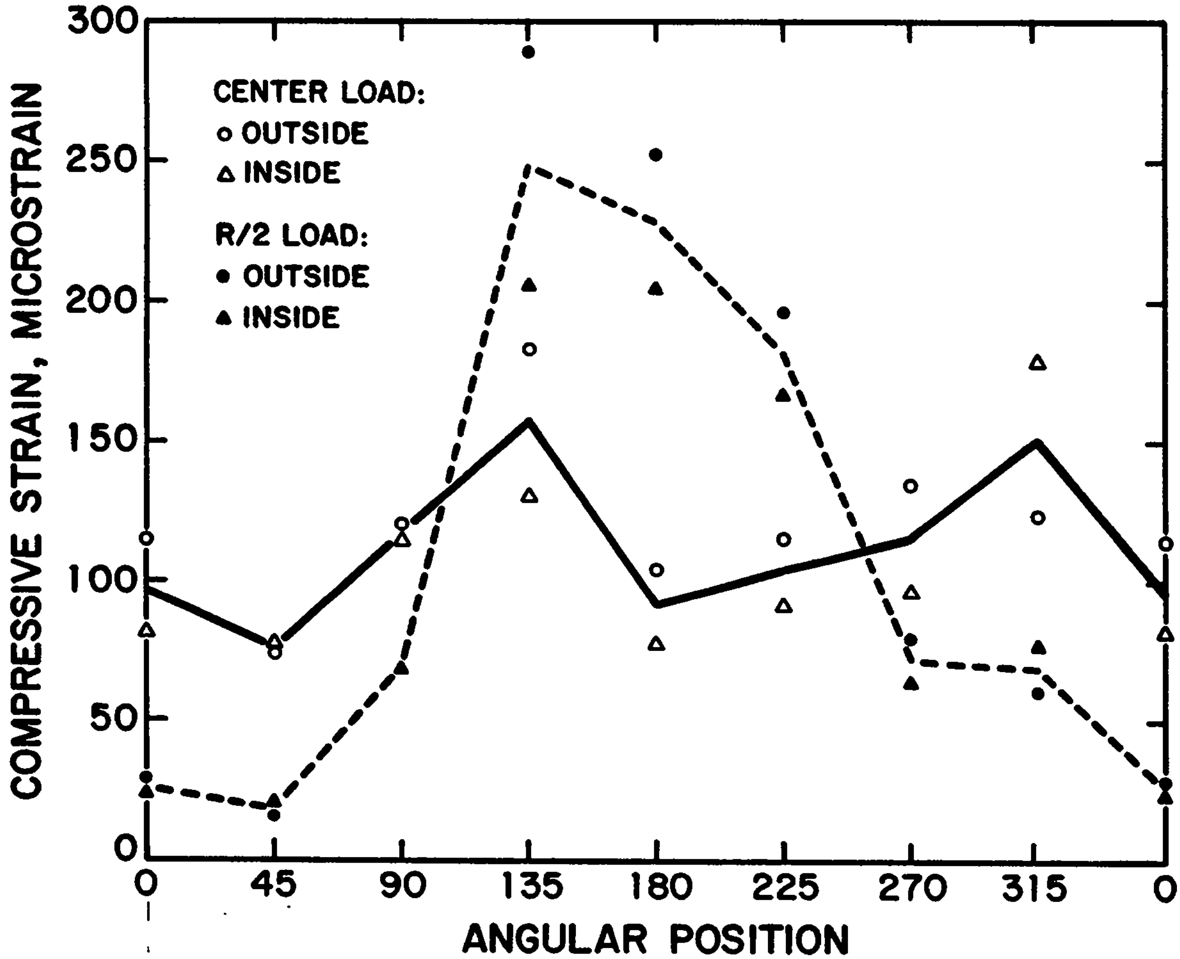

Fig. 26. Strain distribution at 10 000-lb load around base of Model 3.

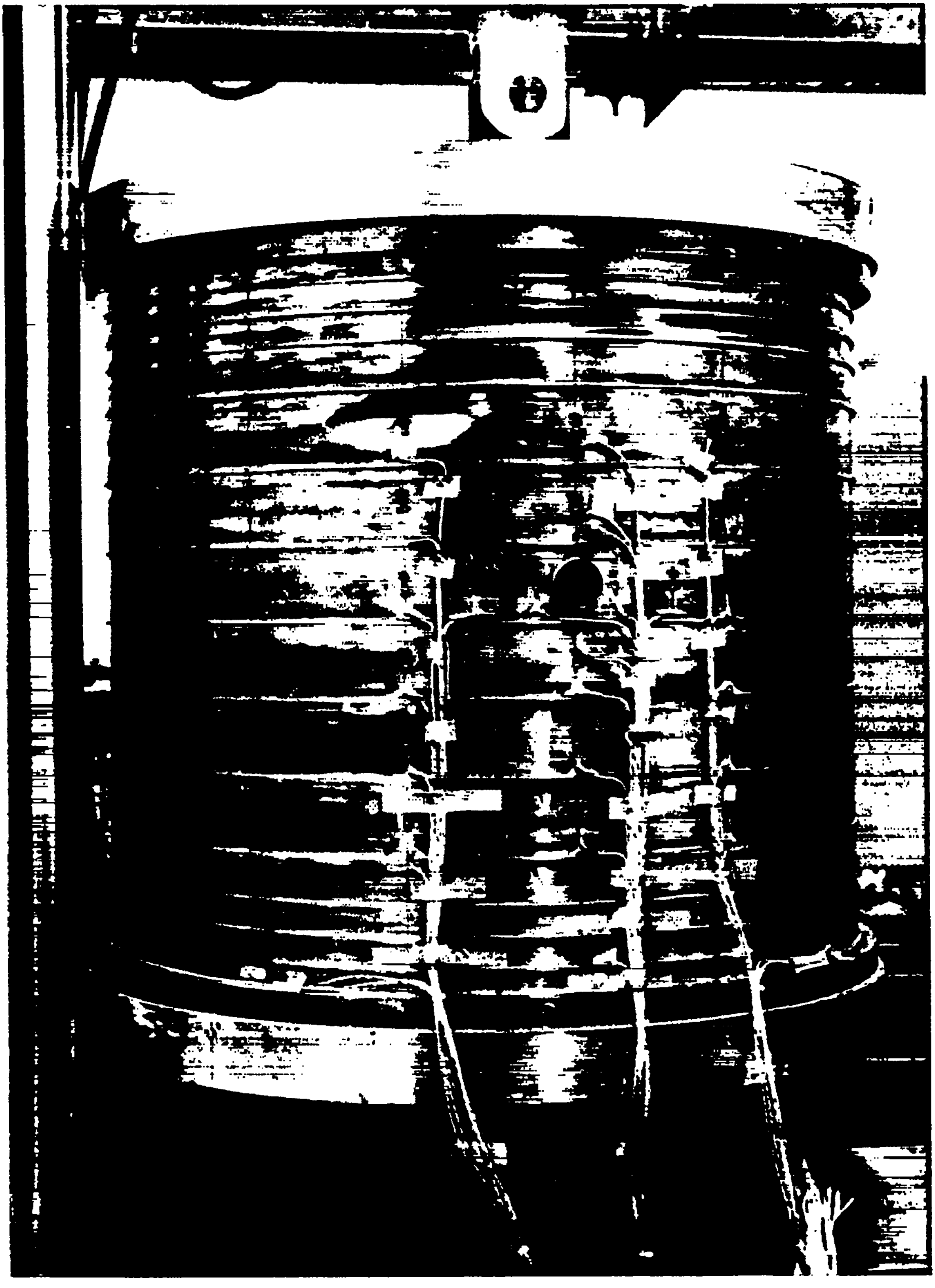

Fig. 27. Buckling deformation of Model 3.

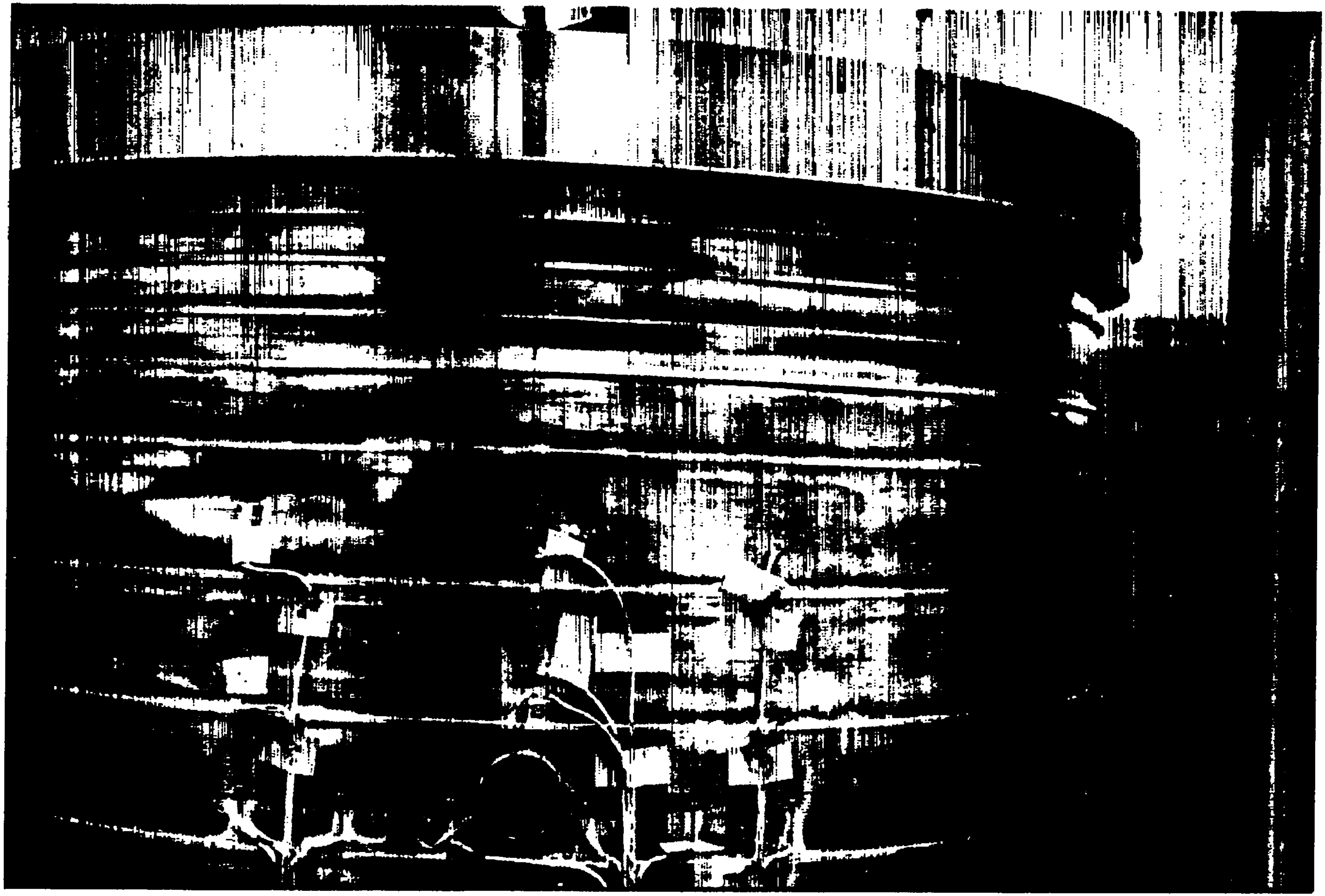

Fig. 28. Close-up of buckling deformation of Model 3.

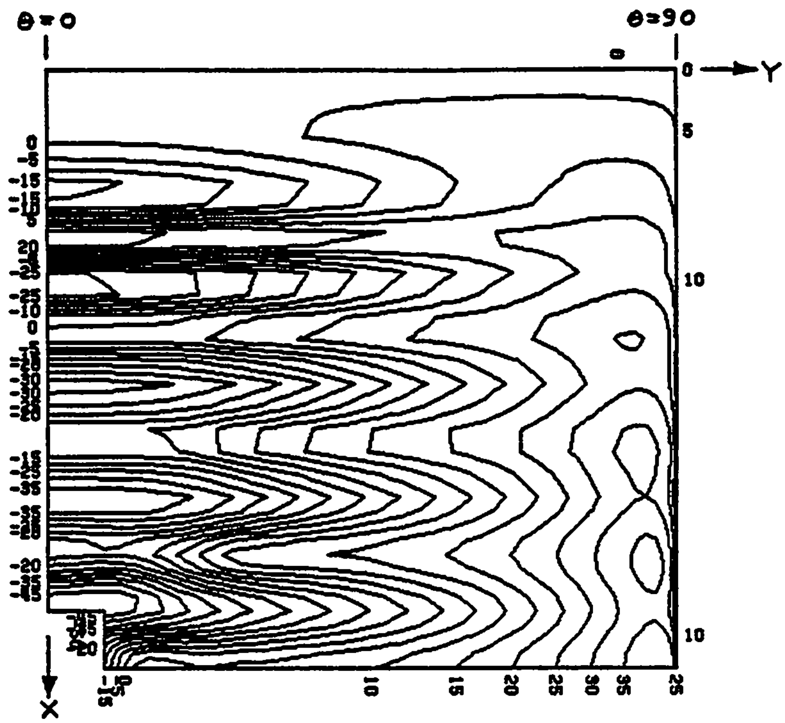

Fig. 29. Buckling contours of Model 3 from analysis by Meller and Bushnell.[7]

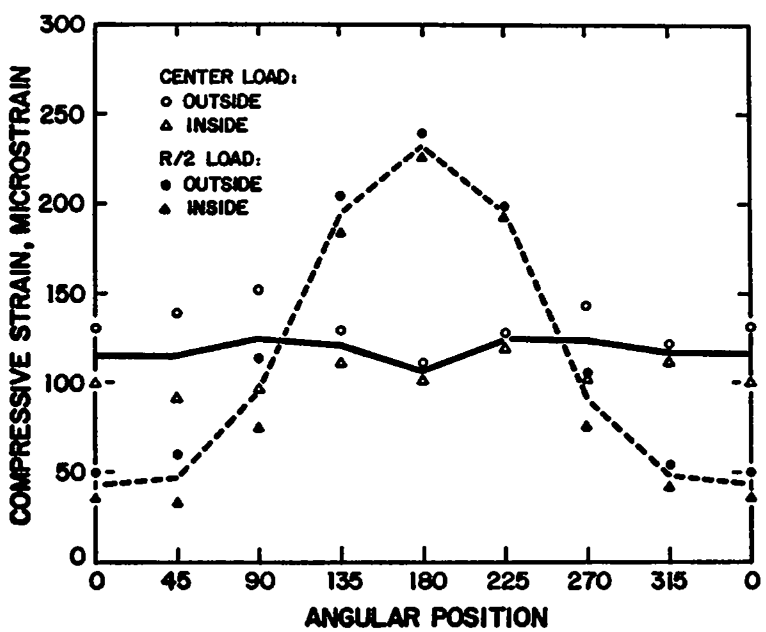

Fig. 30. Strain distribution at 10 000-lb load around base of Model 4.

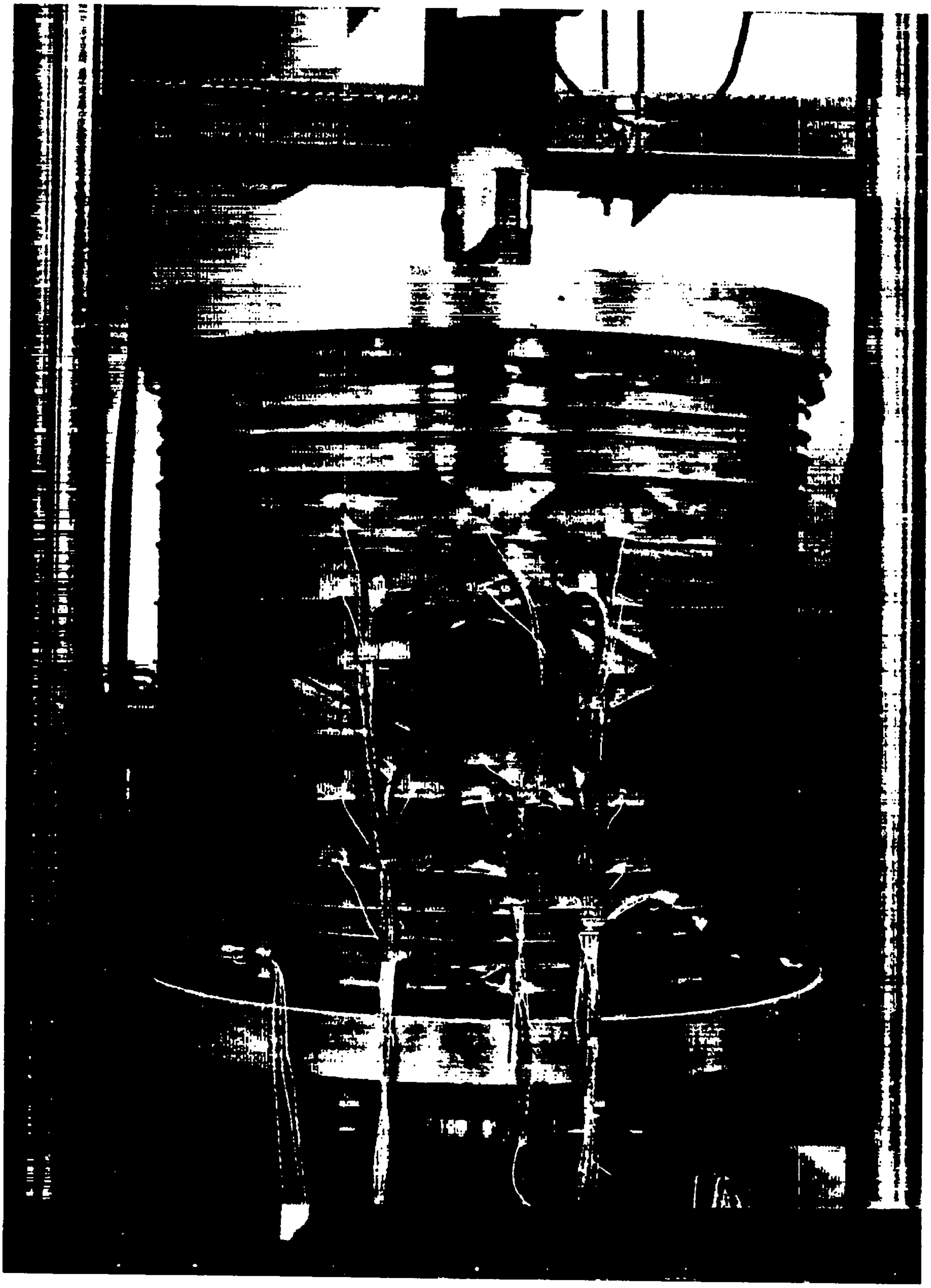

Fig. 31. Buckling deformation of Model 4.

Fig. 32. Close-up of buckling deformation of Model 4.

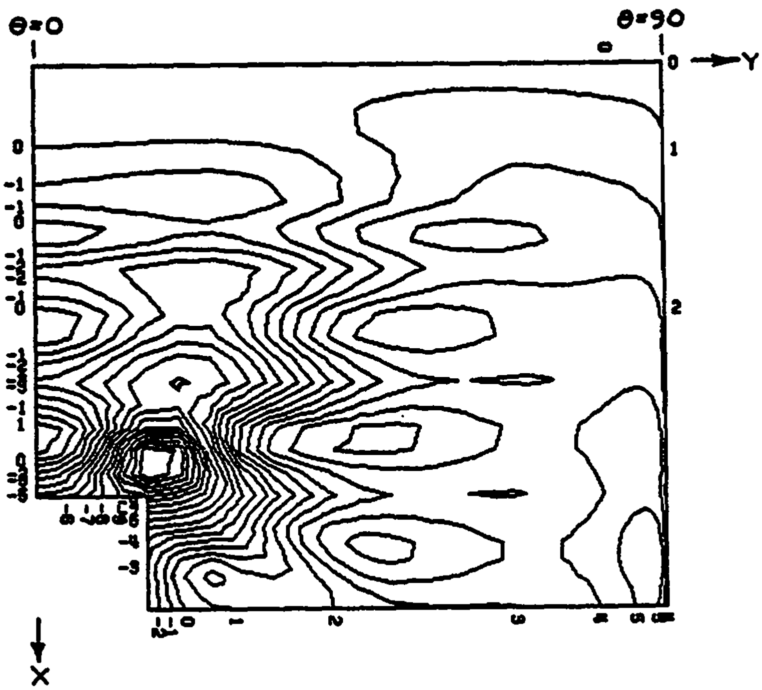

Fig. 33. Buckling contours of Model 4 from analysis by Meller and Bushnell.[7]

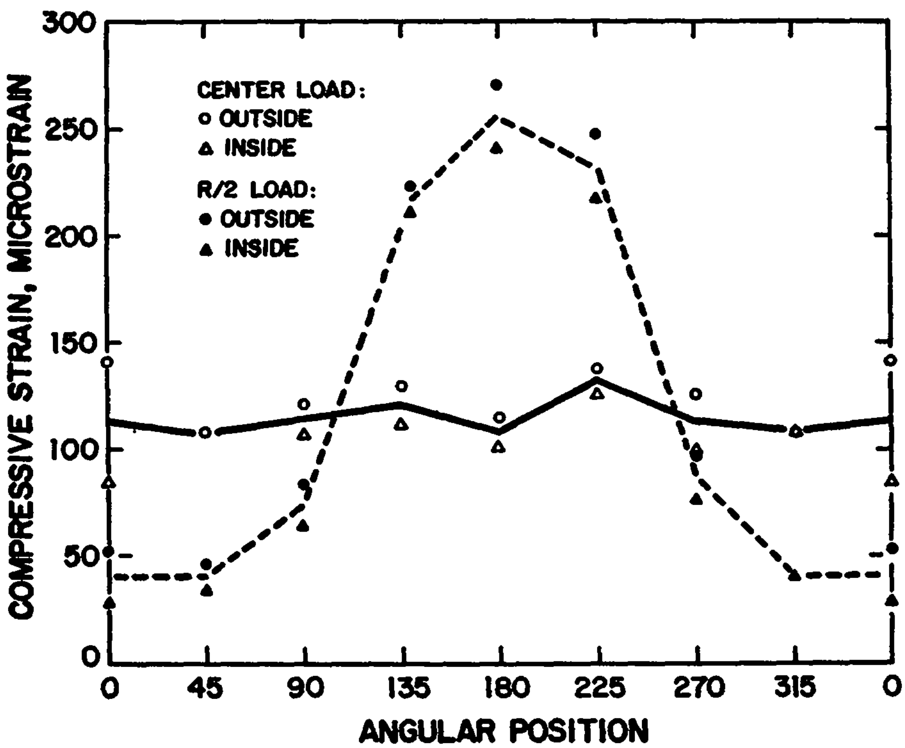

Fig. 34. Strain distribution at 10 000-lb load around base of Model 5.

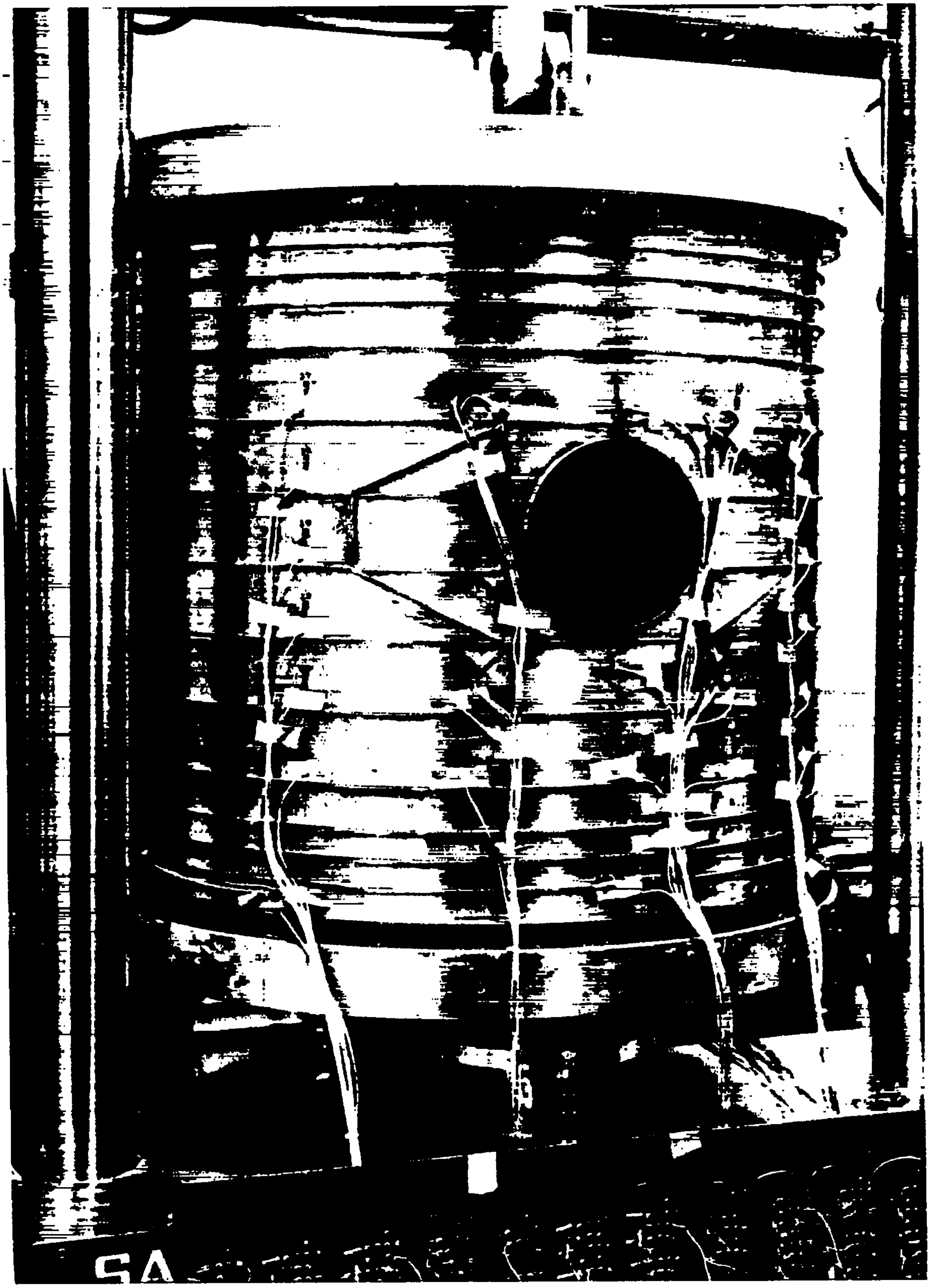

Fig. 35. Buckling deformation of Model 5.

Fig. 36. Close-up of buckling deformation of Model 5.

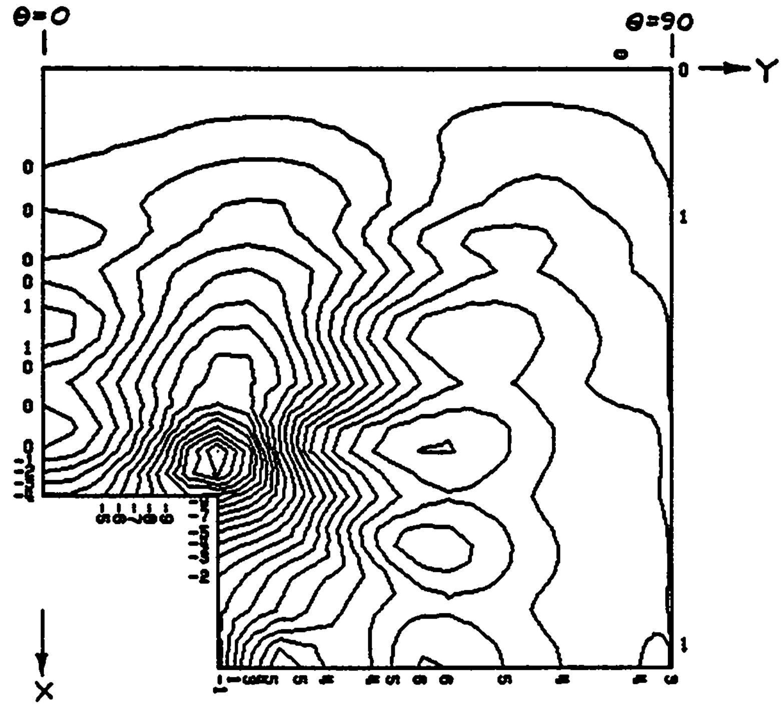

Fig. 37. Buckling contours of Model 5 from analysis by Meller and Bushnell.[7]

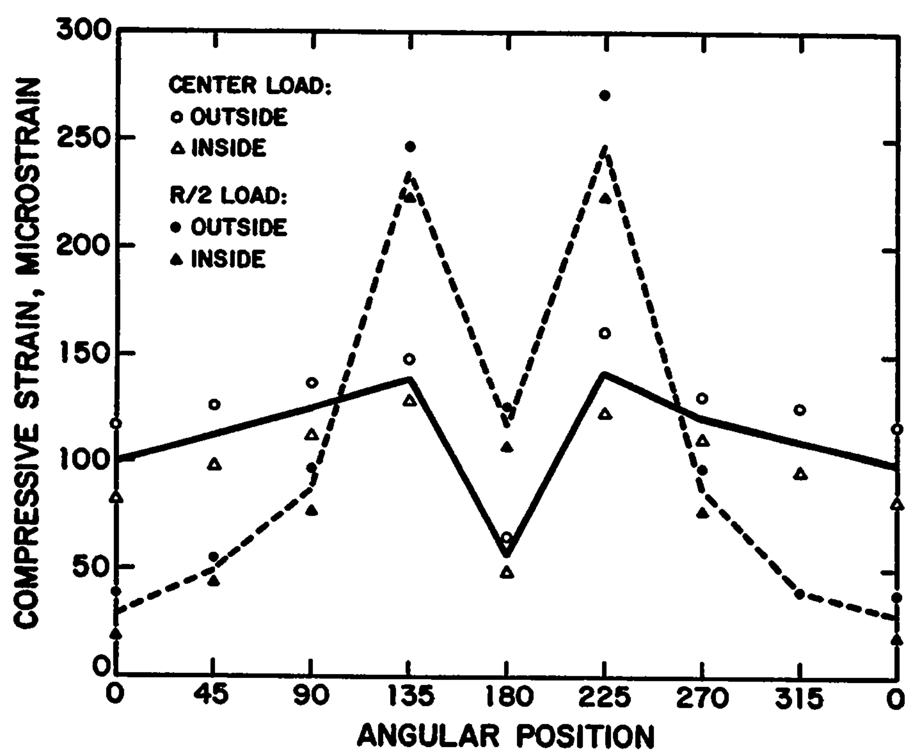

Fig. 38. Strain distributions at 10 000-lb load around base of Model 6.

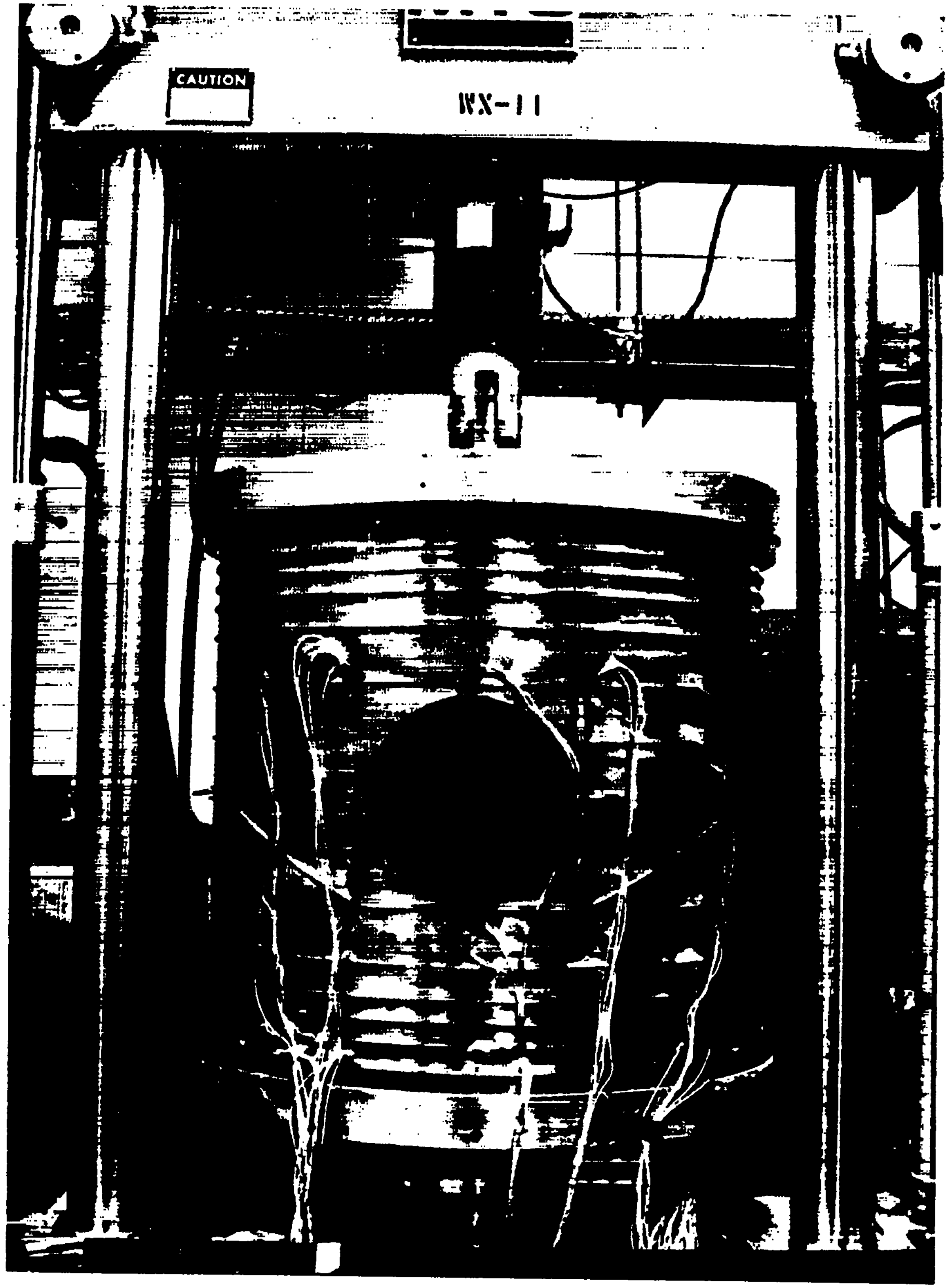

Fig. 39. Buckling deformation of Model 6.

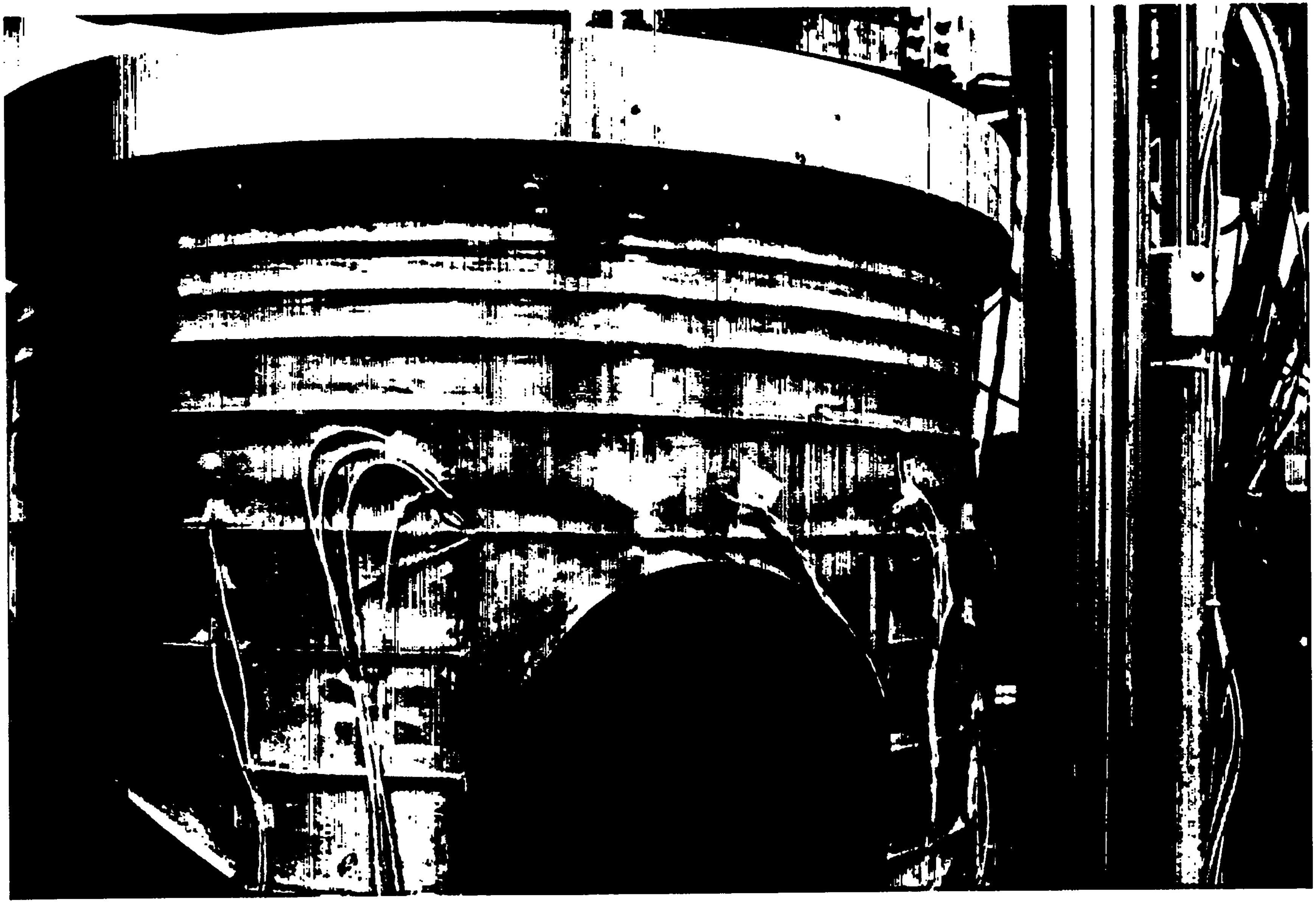

Fig. 40. Close-up of buckling deformation of Model 6.

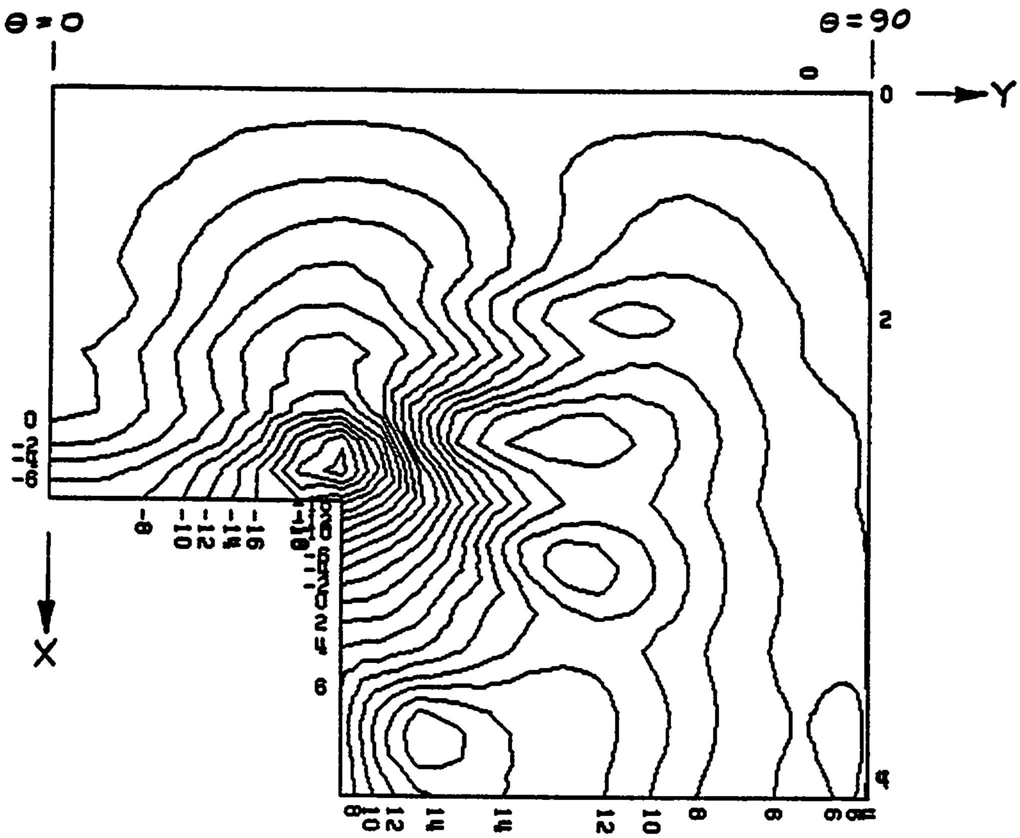

Fig. 41. Buckling contours of Model 6 from analysis by Meller and Bushnell.[7]

DISTRIBUTION

	Copies
Nuclear Regulatory Commission, R5, Bethesda, Maryland	383
Technical Information Center, Oak Ridge, Tennessee	2
Los Alamos National Laboratory, Los Alamos, New Mexico	50
	435

☆U.S. GOVERNMENT PRINTING OFFICE: 1983-0-676-026/12

Available from

GPO Sales Program
Division of Technical Information and Document Control
US Nuclear Regulatory Commission
Washington, DC 20555

and

National Technical Information Service
Springfield, VA 22161

Los Alamos